PSFC/JA-03-29

Impurity Plume Experiments in the Edge Plasma of the Alcator C-Mod Tokamak

S. Gangadhara, B. LaBombard

17 December 2003

Plasma Science and Fusion Center
Massachusetts Institute of Technology
Cambridge, MA 02139 USA

This work was supported by the U.S. Department of Energy, Cooperative Grant No. DE-FC02-99ER54512. Reproduction, translation, publication, use and disposal, in whole or in part, by or for the United States government is permitted.

Submitted for publication to *Nuclear Fusion.*

Impurity Plume Experiments in the Edge Plasma of the Alcator C-Mod Tokamak

S. Gangadhara§, B. LaBombard

M.I.T. Plasma Science and Fusion Center, 175 Albany Street, Cambridge, MA 02139 USA

Abstract.

The physics of impurity transport in response to a local gas injection in the scrape-off-layer (SOL) of Alcator C-Mod is investigated. Carbon "plumes" are formed at variable locations in the SOL – up to the separatrix – by puffing deuterated ethylene gas (C_2D_4) through the end of a reciprocating fast-scanning probe. CCD cameras are used to simultaneously record C^{+1} and C^{+2} emission patterns from two near-perpendicular views. The plume dispersal patterns are found to yield direct qualitative information about plasma flow, including the direction of $v_{\mathbf{E}\times\mathbf{B}}$ near the separatrix. Impurity transport and plasma-surface interaction physics implicit in the 3-D plume structure is explored in detail using a Monte Carlo impurity transport code, with the aim of extracting background plasma-flow quantities. A number of important local effects involving plasma-probe interaction have been identified: a vertical $\mathbf{E} \times \mathbf{B}$ drift near the probe surface, a parallel electric field above the probe tip arising from plasma recycling off the probe surface, and sputtering of a carbon layer that dynamically forms on the probe surface. The emission patterns are also found to yield important information on flows in the SOL: radial electric field ($\mathbf{E}_r$) in the near SOL and volume-averaged values of the parallel Mach number ($M_\parallel$) in the far SOL. $\mathbf{E}_r$ values obtained from plume data compare favorably with estimates of $\mathbf{E}_r$ based on the poloidal propagation velocity of edge plasma fluctuations measured by the scanning probe. Comparisons between parallel Mach numbers obtained from the plume data and probe measurements indicate that the probe over-estimates the parallel flow towards the divertor in the far SOL. This result supports the picture of particle balance in the SOL of Alcator C-Mod being dominated by main-chamber recycling, with weak plasma flow into the divertor.

PACS numbers: 52.25.Fi, 52.25.Vy, 52.25.Xz, 52.40.Hf, 52.55.Fa, 52.55.Rk, 52.65.Pp, 52.70.Kz

Submitted to: *Nucl. Fusion*

§ To whom correspondence should be addressed (sanjayg@psfc.mit.edu).

1. Introduction

Impurity concentration profiles in a reactor will depend on two factors: the source distribution and the transport of impurities in both the core and edge plasma. Impurity transport in the edge plays an especially important role, since it determines the "efficiency" with which impurities generated from divertor and wall surfaces penetrate to the core. Since impurities can be transported by the large $\mathbf{E} \times \mathbf{B}$ and parallel plasma flows which are present in the edge, it is necessary to have an accurate description for the edge plasma flow pattern.

Reciprocating fast-scanning probes are typically used to make measurements of parallel flows ($v_{\|}$) and radial electric fields ($\mathbf{E}_r$) in the scrape-off layer (SOL). Two separate interpretations have been offered for the results that arise from these measurements, which have vastly different implications for impurity dispersal in the edge plasma. The first is based on initial observations made on a number of machines, including Alcator C-Mod [1] and JT-60U [2], of parallel flows in the SOL changing direction near the separatrix, i.e. *reversing* (where the "normal" flow direction is designated as being towards the closest material surface). As these measurements were made in the outboard SOL, they suggested the possibility of a large-scale poloidal flow of the background plasma from outer divertor to inner divertor. Such a flow might provide a mechanism of enhancing impurity concentrations in the core plasma. In addition, a parallel flow of impurities from outer to inner divertor has been suggested as a possible explanation for asymmetries in carbon deposition on the floor of JET [3].

However, more recent results obtained near the outboard midplane on Alcator C-Mod indicate that the poloidal projections of the parallel flow and the $\mathbf{E} \times \mathbf{B}$ flow mostly cancel near the separatrix (where reversed parallel flows are typically observed), tending towards a purely toroidal rotation of the plasma at that location [4]. This interpretation is consistent with results obtained from a model of particle transport in the edge plasma which includes classical drifts [5]. If plasma flows result in toroidal rotation only, then the dominant mechanism remaining for transporting impurities from the divertor plasma into the main chamber SOL (and beyond) becomes the thermal gradient force [6], which is small for typical SOL conditions. This suggests that impurity ions generated near divertor surfaces might in fact be confined to the divertor plasma.

Recent results from C-Mod also indicate that over much of the SOL cross-field transport to the main-chamber walls dominates over parallel transport to the divertor [7]. In this case significant sputtering, and hence impurity generation, from main-chamber walls may be unavoidable. However, this result is based in part on the measurement of small net poloidal flow towards the divertor by scanning probes. Thus, just as with the results discussed above, this conclusion depends on the validity of the probe data. Independent measurements of $v_{\|}$ and $\mathbf{E}_r$ in the edge plasma are therefore desired. In addition, since large flows (including reversed flows) tend to occur predominantly in the near SOL (close to the separatrix), flow measurements in this region are especially necessary.

A conceptually simple means to determine impurity transport and background plasma flows in the SOL is to inject impurities locally in the edge plasma and then "watch" where they go. Experiments utilizing impurity gas injection into the edge plasma from limiter or wall-mounted capillaries have been conducted on a number of machines, including DITE [8], DIII-D [9], TEXTOR [10, 11], and Alcator C-Mod [12]. Results from these experiments are based on visible imaging of the resultant impurity dispersal "plumes" using CCD cameras with bandpass interference filters. From an analysis of the emission structure, parameters which affect local impurity transport can be investigated, and local values of the background flow may be inferred [12].

One important limitation of plume studies conducted using wall-mounted or limiter-mounted impurity injection nozzles is that the resultant plumes tend to be formed close to the wall/limiter, since the ionization mean-free path is shorter than the SOL width for most impurities of interest. Thus, in most cases only the far SOL plasma may be studied, leaving the interesting flow patterns near the LCFS undiagnosed. To address this limitation, a novel diagnostic has been developed on Alcator C-Mod: a gas-injecting fast-scanning probe (FSP) [13]. This diagnostic allows a controlled amount of impurity gas to be injected through the probe tip over a short period near the probe's end-of-stroke. Since the probe scans the entire edge plasma, including up to the LCFS, gas can be injected anywhere in the SOL, allowing plume studies to be conducted as a function of SOL depth. Using two CCD cameras with near-perpendicular views, we have studied C^{+1} and C^{+2} impurity dispersal plumes arising from deuterated ethylene (C_2D_4) injection.

We have found that impurity plume dispersal patterns formed near the separatrix potentially offer critical information about bulk plasma parallel flows and cross-field drifts. In fact, the shape and asymmetry of the plume image often provides direct qualitative information on plasma flow. However, a number of physical phenomena that can influence the dispersal pattern need to be considered before quantitative information on plasma flow can be extracted, including the influence of the probe surface on both the background flow and the life-cycle of the injected impurities. These phenomena are important in themselves and need to be understood, since they are part of the total picture of plasma-impurity-surface interaction physics.

In this article, we present results and analysis from experiments on Alcator C-Mod in which impurity plumes were generated at different depths in the SOL for a variety ohmic L-mode discharges and a few Enhanced D_α (EDA) H-mode discharges. In addition to summarizing the experimental observations, we explore the physics of plume dispersal, the implied background plasma flows, and the implications for edge plasma physics.

A description of the diagnostic is first given in Section 2. A survey of various results from the plume experiments is then presented in Section 3. These results suggest that the impurity emission is vertically elongated along the probe axis, and that emission arising from sputtering of deposited carbon off the probe surface provides a significant contribution to the overall plume structure. In addition, for plumes generated in the

near SOL, the resultant emission contours are observed to be non-elliptical and the parallel extent relative to the ionization mean-free path is found to be large, indicating a "jetting" of impurities along **B**.

The LIM impurity transport code was used to simulate the impurity emission, and is briefly described in Section 4. A physics model for the emission structure is then presented in Section 5. This model features separate components for describing the sputter source of the emission, the mechanism leading to the impurity ion jet, and the cause of the vertical elongation in the impurity emissivity.

In Section 6, results from the plume model are used to extract parallel and cross-field flow information from the emission structure. For plumes generated in the near SOL, estimates of the radial electric field are obtained from an analysis of the jet component of the emission, while in the far SOL estimates of the parallel flow velocity are inferred from parallel asymmetries in the plume emission structure using LIM. Results are consistent with probe measurements which point towards a toroidal rotation of the plasma in the near SOL, but indicate that in the far SOL parallel flows to the divertor are over-estimated by the probe, strengthening the argument for the main-chamber recycling view of SOL particle balance in C-Mod. Finally, in Section 7 the key findings of this work are summarized.

2. Experimental Arrangement

The impurity plume diagnostic consists of two main components: (1) the gas-injecting fast-scanning probe (FSP) and (2) optical views of the probe. The details of each system are briefly summarized below, while a full description of the diagnostic may be found in reference [14].

2.1. Gas-Injecting Fast-Scanning Probe

The fast-scanning probe consists of four tungsten wires embedded in a molybdenum probe head. The wires serve as Langmuir probes, making measurements of local electron density (n_e) and temperature (T_e) in the SOL. A close-up view of the probe head is given in Figure 1. Probe elements are positioned within the probe head such that one pair has directional sensitivity along the local magnetic field line trajectory and the other has directional sensitivity across **B**. In these experiments, the "west" probe looks downstream, i.e. towards the divertor.

The local value of the parallel Mach number ($M_{||}$) may be estimated from the ratio of saturation currents measured on the upstream ("east") and downstream ("west") probes, using:

$$M_{||} = 0.45 \ln \left(\frac{j_{up}}{j_{down}} \right) \tag{1}$$

Equation 1 is based on a 2-D fluid analysis of ion collection by probes in a plasma with background flows and strong magnetic fields [15].

Centered between the probe elements is a 1 mm diameter (i.d.) stainless steel capillary tube. The tube extends down the body of the probe and is connected to a nearby gas plenum. An inertial valve sits inside the capillary near the probe tip, and is designed to open under an acceleration of $\geq$ 30 g's. The acceleration of the probe exceeds this value for a period of $\sim$ 8-10 ms near its end-of-stroke, during which time the probe moves $\sim$ 6 mm, or $\sim$ 4 mm perpendicular to magnetic flux surfaces (based on magnetic equilibria reconstructed from the EFIT code [16]). In the experiments reported here, approximately $\simeq 5 \times 10^{16}$ deuterated ethylene (C_2D_4) molecules were injected per probe scan. Finally, the location of gas injection is mapped to flux surfaces with the cross-field coordinate ρ, corresponding to distance outside the LCFS at the outer midplane ($\rho = 0$ represents the separatrix and $\rho > 0$ the SOL). Values for ρ are typically accurate to within $\pm$ 2 mm.

2.2. Probe views

The resultant impurity emission is imaged from two near-perpendicular views, one from the top of the machine (TVC) and one from the side (SVC). A cross-section of Alcator C-Mod showing the locations of these two views is given in Figure 2. These views are obtained using coherent fiber bundles || optically coupled to gated, intensified CCD cameras through beam-splitters, which allow for the simultaneous acquisition of C^{+1} (CII) and C^{+2} (CIII) emission at each view location (i.e. on each CCD chip). While the overall system yields a spatial resolution of $\sim$ 2.5 mm at the plane of the gas injection location, the final image resolution is in fact $\simeq$ 5 mm for each view, resulting from the use of 9×9 pixel digital smoothing to minimize the contribution from random fluctuations arising from electronic noise.

Images obtained from the fiber bundles are digitized using image-intensified CCD cameras ¶. For typical operation, camera gates are in the range of 0.1-1 ms, minimizing the motion of the probe (0.1-1 mm) during acquisition of a given plume image. A series of calibrations and alignments have been performed to convert the image data to units of brightness ($W/m^2/ster$) and to map this data to field-aligned coordinates. These transformations make it easier to differentiate between parallel and cross-field asymmetries in the emission structure, as well as allow a more direct comparison of experimental data with simulation results, which are generated using a modified version of the LIM impurity transport code [17].

3. Experimental Results

The majority of plume experiments were conducted during a number of ohmic L-mode discharges, in which background plasma conditions spanned the range of line-average densities from 4.0×10^{19} m^{-3} $< \bar{n_e} < 1.4 \times 10^{20}$ m^{-3}, plasma currents from 0.5 MA <

|| Schott Fiber Optics, 122 Charlton Street, Southbridge, MA 01550
¶ Xybion Systems Inc., 8380 Miralani Drive, San Diego, CA 92126

$\mathbf{I}_p < 1.0$ MA, and toroidal magnetic fields from 4 T $< \mathbf{B}_\phi <$ 6 T. Plumes images were also obtained in the near SOL from a few Enhanced D_α H-mode discharges.

3.1. Typical plume data

An example of data obtained from the plume imaging system is shown in Figure 3. Images in the top panel correspond to the side view of the plume (SVC), while images in the bottom panel correspond to the top view (TVC) [Note that the probe obscures the view of the peak emission seen by the SVC; see Figure 2]. In both cases C^{+1} (CII) emission is on the bottom half of the image and C^{+2} (CIII) emission is on the top half. Some simple observations can be made about the characteristics of the emission. First, the plumes are elongated in one direction – this is very clear for the CIII data. The direction of elongation is aligned with the local magnetic field, which is expected since charged particle motion is unconfined along **B**. In addition, CIII plumes have a much longer parallel (to **B**) extent than CII plumes, which is consistent with C^{+2} ions having a longer ionization lifetime than C^{+1} ions.

However, the aspect ratio of the CII and CIII plumes (extent along **B** vs. across **B**) is smaller than one might anticipate based on simple analysis. The cross-field width of the ion emission is (nominally) set by two factors: (1) the neutral source width and (2) the cross-field diffusivity ($D_\perp$). In principle, the width of the neutral distribution is set by the injection capillary diameter (1 mm), while impurity spreading due to diffusion may be estimated as $\Delta \sim \sqrt{D_\perp \tau_{ion}}$, where τ_{ion} represents the ionization lifetime for the charge state of interest. Typical values for $D_\perp$, τ_{ion} (C^{+1}), and τ_{ion} (C^{+2}) in the SOL are $\sim$ 0.1 - 1 m^2/s, 0.2-0.5 μs, and 1-20 μs, respectively, with each parameter increasing in value with distance from the separatrix [7]. Based on these estimates, values for the impurity cross-field width are expected to be $\lesssim$ 2 mm for C^{+1} ions and $\sim$ 1 - 5 mm for C^{+2} ions. These values suggest that the cross-field extent of the observed emission should in fact be set by the optical resolution of the imaging system ($\simeq$ 5 mm) for both CII and CIII plumes. However, this is not the case for most experimental data, in which cross-field widths of order $\sim$ 5-10 mm are found for CII emission and widths of order $\sim$ 10-15 mm are observed for CIII emission. These results suggest that the source width is in fact much larger than 1 mm. One possible explanation is related to the deposition of carbon atoms onto the probe surface, which is discussed below.

Plume emission centroids are also observed to deviate from field lines, and the amount of deviation typically increases with distance (along **B**) from the injection location. This results in plumes which have a "gull wing" or "boomerang" shape, which can be seen in Figure 3 (dashed lines). The deviation is in part caused by a poloidal (in the flux surface) flow of the impurities resulting from the presence of a radial electric field at the injection location (i.e. from an $\mathbf{E} \times \mathbf{B}$ drift). Results from numerical modelling [14] indicate that in the absence of an electric field, an emission boomerang can also arise from the cross-field variation of electron density and temperature (i.e. of the ionization rate). The total plume boomerang is therefore due to both $\mathbf{E} \times \mathbf{B}$

and ionization-rate variation effects. Nonetheless, in many cases the direction of the boomerang can be simply related to the sign of $\mathbf{E}_r$.

As an example, a comparison between CIII SVC plumes formed inside and outside of the Quasi-Coherent (QC) mode [18] layer during a pair of Enhanced D_α (EDA [19]) H-mode discharges is shown in Figure 4. Also shown in this figure are floating potential measurements from the gas-injecting scanning probe (FSP) and a horizontal fast-scanning probe (ASP) located slightly above the outboard midplane in Alcator C-Mod [20] (see Figure 2). ASP results indicate that this probe was located inside the QC mode layer during both discharges, whereas FSP measurements suggest that this probe was located inside the mode layer during only the first discharge (bottom panels). While the plume generated outside the mode layer (top panels) exhibits an emission boomerang consistent with $\mathbf{E}_r > 0$, the plume generated inside the mode layer exhibits a reversed emission boomerang, consistent with $\mathbf{E}_r < 0$. These results suggest that the QC mode exists in a region of ***negative*** radial electric field. The presence of the mode makes it extremely difficult for probe data to be used to infer $\mathbf{E}_r$ – in fact, FSP measurements indicate a *positive* radial electric field when this probe is located inside the mode layer. Thus, plumes may provide the only means of estimating the magnitude of $\mathbf{E}_r$ in this case.

Finally, if the magnitude of ionization-rate variation effects can be estimated, then the boomerang angle can be used to directly estimate the value of $\mathbf{E}_r$. This type of analysis is presented in Section 6.

3.2. Observations of an emission sputter source

As C_2D_4 molecules are injected into the plasma, they are broken up into their constituent atoms with a dissociation mean-free path of $\sim$ 10-20 μm (for typical SOL conditions). Molecular and atomic radicals can be subsequently accelerated towards the probe surface by sheath electric fields and deposited onto the probe head. This material can then be sputtered by the background plasma and again contribute to the plume emission. However, if material is released by chemical sputtering, the resulting hydrocarbon would again be promptly ionized and accelerated towards the probe. Therefore, the dominant mechanism which injects carbon into the plasma is likely to be a physical sputtering process, which imparts sufficient energy to the carbon atoms to allow the resultant ions to escape the influence of sheath electric fields. In this impurity redeposition model, the effective source width of the plume emission would be governed by the probe head geometry, resulting in a cross-field width which is much greater than the injection capillary diameter. This model is consistent with the experimental observations.

Experimental evidence for a "sputter" source exists in the form of a plume generated *without gas injection.* Images of this CIII plume obtained from the top and side views are shown in Figure 5. The plume was generated during the first scan of the probe following a discharge in which C_2D_4 gas was injected through the capillary. The emission brightness in this case is less than but comparable to cases in which plumes are formed

with gas injection, indicating that the contribution of the sputtered plume to the overall emission can be significant ($\sim$ 40-60 %) even when gas is injected.

During the discharge in which no gas was injected, the probe was scanned three times, resulting in three separate sputter-generated plumes. Results indicate that the emission brightness is significantly reduced in the second and third scans, implying that most of the deposited carbon is sputtered off the probe head in one scan (i.e. the probe "cleans up" in one scan). This suggests that the rate of sputtering off the probe head is comparable to the gas injection rate ($\sim 10^{19}$ carbon atoms per second) – if it were much faster, there would be very little carbon left on the probe head to generate a plume during the first probe scan without gas injection, and if it were much slower then the brightness would be both small and of the same magnitude for all three plumes generated from probe scans without gas injection.

3.3. "Jet"-like behavior

Plumes formed in the near SOL also tend to exhibit a "jet"-like feature near the gas injection location, leading to non-elliptical emission contours. An example of this behavior for a CIII image taken from the TVC is shown in Figure 6. The "jetting" action which occurs in these plumes implies that impurities in the vicinity of the probe (in the cross-field direction) travel with high parallel velocity relative to impurities which are further out. In addition, the parallel extent of the emission is much longer than the ionization mean-free path estimated from local measurements of n_e and T_e in these cases. This suggests the existence of a mechanism which imparts significant parallel energy to the impurities in the near SOL. A plausible mechanism identified by numerical modelling is the presence of a localized parallel electric field at the gas injection location, which arises as a result of background ion recycling off the probe head. This phenomenon is discussed in more detail in Section 5.3, and provides a means to infer the $\mathbf{E} \times \mathbf{B}$ flow near the separatrix (Section 6).

CIII TVC plumes which exhibit little ("transition") or no jet-like behavior are also shown in Figure 6 for comparison. Qualitative characterization of the plume data into "jet", "transition" and "no jet" categories has been used to explore correlations between plume structure and background plasma conditions. An example of these results is shown in Figure 7, in which electron temperature (as measured by the FSP) is plotted against SOL depth for all discharges in which plumes were generated. Unfortunately, there happens to be large scatter in the temperature data acquired during these particular discharges (caused by intermittent shorting of the probe). Nonetheless, the results indicate that the apperance of "jet"-like structure in the emission data predominantly occurs for plumes formed close to the separatrix, where values of T_e are large ($\sim$ 50 eV).

3.4. SVC/TVC plume width asymmetry

For the majority of CIII plumes collected, the cross-field extent of the SVC data is found to be larger than the cross-field extent of the TVC data. CIII brightness values are also observed to be somewhat larger for TVC plume data than for SVC plume data, indicating that the signal on each TVC pixel arises from integration through a larger amount of emission. These results suggest that the C^{+2} emission is vertically elongated (i.e. extends down the probe axis).

A comparison between 1-D cross-field profiles of CIII SVC and TVC emission data for a plume formed in the near SOL is given in Figure 8 (top panel). In this case the profiles were generated by integrating the corresponding 2-D brightness data over a limited extent along $\mathbf{B}$ (-2.5 cm $\leq x_{||} \leq$ -1.5 cm). The results indicate that the absolute brightness observed by the TVC is larger than that observed by the SVC in this case. In addition, for cross-field distances greater than $\simeq$ 2 cm away from the injection location, the TVC data exhibit unexpected behavior, such as an increase in the brightness with increasing distance towards the core of the plasma (i.e. with decreasing R). This behavior is thought to be caused by the presence of structure in the background emission which results from reflections off invessel component surfaces. However, data at brightness levels which are small relative to the peak ($\lesssim$ 10-15%) are typically neglected in the analysis of the plumes (see Section 4).

A comparison between the normalized brightness profiles for the two views is shown in the bottom panel of Figure 8. Ignoring data in the far field ($\gtrsim$ 2 cm away from the injection location across $\mathbf{B}$), good agreement is observed between the results for the region of plasma towards the core (increasing Z, decreasing R). However, in the region of plasma away from the core, the SVC profile is skewed relative to the TVC profile, indicating that the plume is extended in the vertical direction. This result confirms that CIII emission is elongated along the probe axis.

Possible explanations for the vertical elongation of the CIII plumes have also been investigated using numerical modelling. The results suggest the presence of a vertical $\mathbf{E} \times \mathbf{B}$ drift for the impurity ions, which is caused by the presence of a local electric field arising from the variation of probe-induced presheath potentials. This is discussed further in Section 5.1.

4. Plume Modelling

Although simplified 1-D & 2-D analytic fluid modelling has been used to provide a basis for intuitive understanding of the plume data [14], to realistically simulate the plumes the full set of mass, momentum, and energy equations need to be solved. Here we utilize a resource that was developed for studying impurity transport in SOL plasmas, namely LIM [17].

4.1. Code Overview

LIM (Limiter Impurity) is a 3-D Monte Carlo impurity transport code. Particles may be "launched" into the plasma as either neutrals or ions ("launch" referring to the specification of the particle position and velocity vectors at its time of origin); they are followed from their point of origin until they exit the plasma by striking a wall or limiter. The coordinate system in LIM is cartesian, where y represents the distance along the magnetic field, x represents the radial cross-field coordinate, and p represents the poloidal (in the flux surface) cross-field coordinate. Finally, although individual particles are followed, they each represent an ensemble of impurity ions with average velocity and temperature.

The transport of impurity ions along field lines is assumed classical, and is governed by coulomb collisions with the background plasma according to three characteristic time constants [17]. These parameters depend on local values of the background density and ion temperature (where $T_i = T_e$ is assumed for plume simulation), which are specified as code inputs based on FSP measurements. Conversely, the cross-field transport of impurity ions is modelled as anomalous, and governed by the following transport coefficents, all of which are specified as inputs: D_p, D_x, v_p, v_x. Other inputs to the code are the parallel flow velocity and the parallel electric field. These may be specified at each individual computational cell, though in general, functional forms are used to generate their values.

Outputs from the code include 3-D spatial distributions for each charge state, 3-D spatial variations for the total radiated power, and the average ion temperature of each charge state "cloud". Spatial distributions of each charge state may be converted to number density (m^{-3}) by specifying an injection rate for the impurities, which for the plume experiments is known. Density in turn may be converted to emissivity using photon emissivity coefficient (PEC) data, which is obtained from the ADAS database [+]. Finally, a 2-D brightness at each experimental view location can be calculated from the 3-D simulated emissivity by *"virtual imaging"* of the emission, allowing the numerical results to be compared directly with experimental data [14].

4.2. Code modifications

A number of modifications have been made to the code to provide a more accurate simulation of the plume experiments. These include allowing for the specification of a non-poloidally symmetric limiter surface, so that an appropriate representation of the probe geometry can be given in the code, as well as the implementation of a presheath model (based on a modified version [21] of the 2-D fluid model of Hutchinson [15]) to describe the variation of background plasma parameters on field lines that intersect the probe surface. However, simulation results indicate that neglecting the presheath does not significantly change the plume dispersion (apart from providing a mechanism for

[+] H.P. Summers. Atomic Data and Analysis Structure (ADAS). **http://adas.phys.strath.ac.uk/**

carbon deposition on the probe surface), since most of the impurities are on field lines which do not intersect the probe. Thus, the final plume results are insensitive to the specific details of the presheath model which is implemented in the code.

Models have also been developed to describe carbon sputtering and background ion recycling off the probe surface. Carbon sputtering is modelled by launching carbon neutral atoms from the probe surface with a Thompson energy distribution [22] (characterized by a surface binding energy U_0, which is specified as an input parameter), while deuterium recycling is modelled by launching deuterium neutral atoms from the probe surface with fixed energy (= 3 eV, given by the Frank-Condon dissociation model [23]) into a fixed plasma background. In the latter case, the step associated with dissociation of the D_2 molecules actually formed by ion recycling has been neglected, under the assumption that the D_2 dissociation mean-free path is much smaller than the D^0 ionization mean-free path (true for most SOL conditions). In both models the probability of a neutral being launched some distance down the probe axis is assumed to decay exponentially with distance – for ion recycling the decay length is determined from the experimentally measured saturation current profile, while for carbon sputtering it is simply specified to provide the best match between simulation and experiment. More details on the launch dynamics may be found in reference [14].

Charge exchange is also included in the ion recycling model. The primary effect of charge exchange is to increase the neutral mean-free path, which in turn increases the volume over which ionization of the recycling deuterium atoms takes place. This volume plays a role in determining the magnitude of the resultant density perturbation and thus the effect of recycling on the injected impurity ions. Finally, absolute values for the D^+ densities which arise from ion recycling are determined by multiplying the simulation results by the true injection rate. In steady-state, the injection rate of deuterium atoms is equal to the collection rate by the probe, which again may be calculated from saturation current measurements.

5. Plume Physics Model

A physics model for the emission structure has been developed using LIM to simulate plumes generated in both the near and far SOL. This model, which is able to reproduce the parallel and cross-field extents of the emission as well as the vertical elongation of the plumes, is described below.

5.1. SVC/TVC plume width investigation

A comparison between 1-D cross-field profiles for the SVC and TVC suggests that the impurity density distribution is vertically elongated, implying that a mechanism exists to transport impurity ions down the probe axis. A number of possible explanations for this phenomenon were investigated using LIM. These include effects of carbon recycling off the probe surface and the presence of a vertical ion drift velocity.

5.1.1. Carbon recycling model Gas injection through the scanning probe results in the formation of a carbon layer over an unknown fraction of the probe surface. However, a rapid removal of this deposited layer is observed when the probe is scanned into the plasma without gas injection. This indicates that the carbon layer results from a dynamic balance between deposition and sputter erosion. Therefore, it may be appropriate to consider a situation in which the carbon concentration on the probe surface is approximately constant in time, i.e. that during gas injection a steady-state is reached. In such a case, for each carbon ion which is absorbed onto the probe surface a carbon neutral is released. This "100% recycling" model is expected to significantly increase the effective lifetime of a given carbon atom, which may allow diffusion to play a significant role in transporting impurity ions down the probe axis.

A recycling model for carbon impurity ions was implemented in LIM based on a steady-state assumption. In this model a carbon ion which is absorbed onto the probe surface is re-launced as a neutral, with an energy given by a Thompson distribution [22]. A pair of simulations were then conducted with and without carbon recycling to determine the effect of recycling on the impurity dispersal. In both cases the cross-field diffusivity was set equal to 1.0 m^2/s, while density and temperature profiles characteristic of the near SOL were used as inputs. A comparison between the resulting 2-D CIII SVC plumes indicates that the parallel extent of the emission is increased when recycling is included, due to a 40% increase in the effective carbon lifetime, but that the cross-field width of the emission exhibits little change. Additional studies performed with larger values of $D_\perp$ suggest that this parameter has a small effect on the results. Thus, the vertical extent of the plumes is not affected by carbon recycling under these conditions.

5.1.2. Probe-induced $\boldsymbol{E} \times \boldsymbol{B}$ drifts Another possible mechanism for transporting carbon ions down the probe axis is a vertical ion drift, which may be induced by the presence of the probe. Specifically, near the probe surface large gradients in the plasma potential exist due to the presence of the probe-induced presheath. Estimates derived from presheath modelling suggest that the potential can vary by $T_e/2$ over a cross-field distance corresponding to the probe radius. In the near SOL ($T_e \simeq 50$ eV) this leads to a local electric field of $\simeq$ 3-4 kV/m. The field is directed towards the region of presheath density depression caused by the probe, resulting in an $\mathbf{E} \times \mathbf{B}$ drift which circulates around the probe. A schematic of the probe geometry indicating the direction of both the field and the resultant drift, as well as the possible effect of such a drift on the impurity ion distribution, is shown in Figure 9. For typical values of the magnetic field strength at the probe location ($\simeq$ 4 T), the $\mathbf{E} \times \mathbf{B}$ velocity is $\simeq$ 750-1000 m/s, which is quite substantial.

LIM has been configured to include a constant drift down the axis of the probe in the region of the plasma below the injection nozzle. Although this velocity field does not have the circulating pattern shown in Figure 9, it can be used to investigate the possible influence of probe-induced $\mathbf{E} \times \mathbf{B}$ drifts on the impurity ion distribution. A

simulation was then conducted in which the drift velocity down the axis of the probe was set equal to 1000 m/s, $D_\perp$ was set equal to 1.0 m^2/s, density and temperature profiles characteristic of the near SOL were used as inputs, and carbon recycling off the probe surface was included. For this case, a comparison between simulated and experimental 1-D cross-field profiles of normalized brightness for both the SVC and TVC is also given in Figure 9. Although relatively good agreement between simulation and experiment is observed, in order to get the simulated SVC plume to have a skewness which is similar to the experimental data it is necessary to postulate a relatively constant electron density profile in computing the CIII excitation rate.

This result is not necessarily inconsistent with the probe measurements. At each location in the SOL, the probe measures the value of electron density at its tip, while values of n_e further down the axis are unknown. If a large $\mathbf{E} \times \mathbf{B}$ drift is responsible for transporting impurity ions formed near the probe tip down the probe axis, this drift will also result in the transport of bulk plasma ions down the probe axis, since $\mathbf{E} \times \mathbf{B}$ drifts are the same for all ion species. Therefore, this drift will affect the electron density along the probe axis, and can result in a uniform distribution. The effect is consistent with the formation of a carbon layer over a finite extent of the probe surface.

5.2. Sputter source model

The drift and surface layer formation models implemented in LIM are rather basic, and are not capable of exploring the influence of the resultant $\mathbf{E} \times \mathbf{B}$ flow patterns on impurity and bulk plasma transport in a self-consistent way. Therefore, a simple model has been developed to account for the contribution from sputtering of carbon deposited on the probe surface to the overall plume emission. Two input parameters are used in LIM to characterize this sputter source: λ_{ss}, which represents the exponential decay length down the probe axis for the sputter distribution, and U_0, which represents the surface binding energy of the carbon atoms. Values for U_0 are difficult to determine, because very little information exists on the surface chemistry for carbon atoms deposited on molybdenum. However, for sputtering of carbon from a graphite surface, $U_0 = 7.4$ eV [24]. Binding energies in the range of a few eV are therefore expected.

The sputter source model has been demonstrated to provide a reasonable simulation of plume emission in the far SOL. An example of this is shown in Figure 10. For this case $\lambda_{ss} = 10$ mm, $U_0 = 5$ eV and $M_{||} = -0.18$ (constant over the emission volume). In the top panel a comparison between experimental and numerically generated 2-D CIII TVC plumes is given, while in the bottom panel a comparison between the corresponding 1-D parallel emission profiles is shown. The main difference is the emission structure in the near field (close to the injection), where reflections off the probe head result in the experimental emission being peaked. In the far field ($\gtrsim 2$ cm away from the injection location along $\mathbf{B}$) the parallel decay lengths are approximately equal, indicating good agreement for the parallel extent between simulation and experiment. Good agreement is also observed between the simulated and experimental values for the cross-field width,

which are within 12% in this case. These results suggest that a sputtering launch-energy distribution is an appropriate model for plumes generated in the far SOL plasma.

The sputter source model is also able to reproduce the cross-field extent of plumes generated in the near SOL. However, this model is unable to re-create the "jet" seen in the experimental data in these cases, the presence of which leads to broad parallel emission profiles. To generate the same parallel extent in the simulation results without creating a jet, a large value for the binding energy is required ($U_0 = 20$ eV), resulting in the average speed of impurity ions away from the injection location being large. This value of U_0 is unreasonable, given the value for the surface binding energy of carbon on graphite.

A study was conducted to investigate whether in this case the parallel extent of the emission could be explained by inaccurate background plasma measurements rather than an unrealistic value of U_0. In other words, are the density and temperature values measured by the scanning probe (and subsequently inputted into the simulation) too large? However, results indicate that in the near SOL the parallel extent of the simulated emission is rather insensitive to values of n_e and T_e (when reasonable values of U_0 are used – see reference [14]), suggesting that probe measurement errors are in fact not responsible for the inability of the sputter source model to simulate the parallel extent of plume emission generated in this region.

5.3. Possible causes for jet behavior

The general conclusion is that the parallel velocity of impurity ions away from the probe must be large in order to explain the parallel extent of the emission. Estimates for this velocity may be obtained from the experimental data by assuming that the peak brightness at each parallel coordinate in a 2-D plume image is dominated by emission from the jet. The ionization lifetime of impurities in this region is first calculated using local values of n_e and T_e. The average parallel velocity ($\bar{v}$) of these impurities is then calculated by dividing the average parallel decay length of the jet by the ionization lifetime. An example of such a "ridge-line analysis" performed for a CIII TVC plume is shown in Figure 11. Results indicate that the parallel velocity obtained from such calculations is indeed quite large, of order the impurity ion sound speed ($\sqrt{T_e/m_z}$, where m_z is the impurity ion mass).

A mechanism other than sputtering must therefore exist to provide "directed" parallel energy to the impurity ions. In addition, it must be a collisionless mechanism, since coulomb momentum transfer rates are small for C^{+2} ions present in conditions typical of the near SOL. Finally, since the impurity ions must have a directed flow away from the probe, it is reasonable to assume that this energy-transfer mechanism does not exist in the background plasma in the absence of the probe. Thus perturbations resulting from plume formation, either due to gas injection or to the probe itself, were investigated as possible mechanisms which might give rise to the jet.

Calculations which employ a simple energy balance indicate that T_e is unaffected

by impurity gas injection. Conversely, results obtained from a simple particle balance suggest that a significant density perturbation can arise as a result of gas injection into the near SOL plasma [14]. For example, for a carbon injection rate of 10^{19} atoms/second, the resulting electron density perturbation can be as large as $\sim 6.5 \times 10^{19}$ m^{-3}, which is a considerable fraction of the background density. However, perturbations arising from the presence of the probe are expected to be even more important.

As a result of the pyramidal probe head geometry, one anticipates that the recycling flux of neutrals from the probe surface will appear predominantly on field lines which do not intersect the probe. The ionization of neutrals on these field lines might cause the formation of a localized density perturbation. This process is illustrated schematically in Figure 12. Results from a simple particle balance suggest that the density perturbation can be a factor of 4 or more larger for background ion recycling off the probe surface than for gas injection.

However, for both gas injection and recycling, the resultant ionization source is localized near the probe, implying that in the far field the density might be considerably lower. A variation of density along **B** would lead to a variation in the plasma potential, assuming that density and potential are related by a Boltzmann relationship: $n_e \propto e^{-e\phi/T_e}$. This variation would result in the generation of a parallel electric field, present on field lines that do not intersect the probe and directed away from the probe. This mechanism could provide impurity ions present near the probe tip with "directed" parallel energy away from the probe. The parallel velocity of these ions would therefore primarily be determined by $E_{\|}$ and not thermalization with the background plasma. For a sufficiently large parallel electric field, the plume would be extended in the parallel direction.

5.4. D^+ plume arising from D_2 recycling

LIM was configured to investigate the magnitude of the density perturbation and resultant electric field caused by local recycling. A typical result from the deuterium recycling simulations is given in Figure 13, in which surface plots of the total electron density (background plus recycling-induced) are shown for two radial coordinates: $x = 0$ mm and $x =$ -2 mm. The location of these surfaces with respect to the probe geometry is also illustrated schematically in this figure. Background density and temperature profiles characteristic of the near SOL were used as inputs to the simulation for this case. LIM output were scaled to absolute units (m^{-3}) using a typical experimental value for the recycling rate, taken to be 2.6×10^{20} atoms/second. Effects arising from density variation in the presheath have also been included. Finally, note that these results are based on the use of a perturbative analysis, i.e. one in which the background conditions are not affected by recycling. The use of such an analysis is found to be reasonable based on results presented in reference [14].

The observation of strong density peaking in the poloidal coordinate (p) suggests that the recycling perturbation occurs predominantly on field lines near (but not

connected to) the probe surface. The poloidal density asymmetry observed on the x = -2 mm flux surface results from the variation in recycling flux with distance down the probe axis (as a result of the probe axis being tilted with respect to flux surfaces; see Figure 2). For the flux surface at $x = 0$ mm, the density perturbation is highly localized to the field line which passes above the probe tip. In addition, the perturbation on this field line is quite large, leading to a parallel variation in the plasma potential which is of order the electron temperature (assuming n_e and ϕ are related by a Boltzmann relationship). This variation is consistent with results obtained from a ridge-line analysis of the experimental data, which suggest that C^{+2} ions must be accelerated up to the impurity ion sound speed by the parallel electric field in order to explain the parallel extent of the jet. The localization of the density perturbation in the cross-field coordinate is also consistent with the small cross-field extent observed for the jet-like region of the experimental emission.

In the far SOL the recycling perturbation is found to be small in LIM, consistent with the observation of little or no jet-like behavior for plumes formed in this region. In general, since $E_{\|}$ is a result of a localized density perturbation, its magnitude is thought to be related to the ionization volume for the recycling deuterium neutrals, which depends on the ionization mean-free path for these neutrals. In Figure 14, normalized potential drops versus neutral mean-free paths are shown for both experimental data and for LIM simulations. The experimentally-derived potential drops are calculated from values for the average ion velocity in the jet ($\bar{v}$) using an energy balance (and assuming an initial energy E_0 of 3 eV for the C^{+2} impurity ions), whereas the LIM-derived values for $\Delta\phi$ are calculated directly from the density perturbation results (using the Boltzmann law). The experimental data exhibit a strong variation of the recycling perturbation strength with the ionization mean-free path. However, in LIM the trend is observed to be weaker, and suggests that a finite level of perturbation exists even in the far SOL. Reasons for the discrepancy between experimental and simulated results are unknown, although the lack of a self-consistent recycling calculation in LIM (i.e. one in which the effects of the recycling perturbation on the background plasma conditions are accounted for) could result in simulated values being too large. Nonetheless, the general trends are similar for experiment and simulation, indicating that the recycling perturbation is indeed a likely cause for the jet-like behavior of impurity plumes formed in the near SOL.

5.5. Jet model for near SOL plumes

A model has been developed in LIM to include the effects of a density perturbation in the simulation of impurity dispersal in the near SOL.

5.5.1. Parallel Electric Field Parallel electric fields inputted into LIM are the result of recycling perturbations ($E_{\|,pert}$) as well as probe-induced presheath effects ($E_{\|,ps}$). While $E_{\|,ps}$ exists on field lines which are connected to the probe, $E_{\|,pert}$ is present only

on those field lines outside the presheath.

Due to computational limitations which constraint the number and size of additional inputs to the code, the full 3-D structure of $E_{\|,pert}$ could not be used in LIM. A 1-D approximation to the field was instead employed to simulate jet-like behavior in the plume emission, under the assumption that emission from the jet is predominantly due to impurity ions which form as a result of direct injection rather than from a sputter source, and that the parallel electric field in the jet therefore has negligible cross-field variation over the extent of the impurity source. The inputted 1-D $E_{\|,pert}$ profile was taken to be the profile on the field line passing above the probe tip. In addition, to increase the parallel resolution of this inputted field and to smooth out statistical fluctuations, an analytic function was used to fit $E_{\|,pert}$, which is linear in the near field (close to the injection) and exponential in the far field.

Tests have been conducted which indicate that the far-field behavior of the C^{+2} impurity ions is relatively insensitive to the structure of $E_{\|,pert}$, but is instead primarily dependent on the total potential drop experienced. Since the parallel extent of the experimental emission is characterized only by the far-field behavior (the near-field behavior is thought to be influenced by the presence of probe head), for experimental plume simulation only the total potential drop implied by deuterium plume modelling is therefore used to determine the parallel electric field.

5.5.2. Modelling results An example of an experimental CIII TVC plume generated in the near SOL is shown in Figure 15. To simulate this plume, two components of the emission are summed together with equal weight: one arising from a localized launch of impurities (representing the source due to direct gas injection) into a background plasma containing the recycling-induced parallel electric field (cumulatively known as the "jet" model for the plume emission), and one arising from a sputter source launch into a nominal (no $E_{\|,pert}$) plasma background (i.e. using the sputter source model). Using parallel electric fields consistent with the magnitude of the recycling perturbation to simulate the first emission component, the resulting composite plume is also shown in Figure 15.

There remains structure in the near field which has not been reproduced, i.e. the non-elliptical shape of the emission contours. This may be due to the inability of the numerical modelling to simulate the effect of reflections off the probe head. It may also be a result of the inability of the numerical modelling to include the 3-D structure of the recycling-induced parallel electric field. The influence of the true 3-D parallel electric field on sputter-launched impurities might be to stretch the plume emission contours along field lines passing near the probe tip while leaving emission contours on field lines away from the probe tip unaffected – a process that might generate the non-elliptical emission contours which are observed experimentally.

Nonetheless, both the cross-field width and the parallel extent of the simulated emission compare reasonably well with the experimental results. This is confirmed by comparing inverse decay lengths for the simulated 1-D parallel emission profile against

the corresponding values for the experimental parallel emission profile (both profiles are shown in Figure 15, bottom panel), which are found to agree within $\simeq$ 10%, and by comparing values for the average cross-field width of the experimental and simulated plumes, which are found to agree within $\simeq$ 20%. These results suggest that the sputter source and jet models for the plume emission provide appropriate descriptions for the physics of impurity ions injected into SOL plasmas via the FSP.

5.6. Parallel flow effects

In the near SOL weak collisional coupling exists between C^{+2} and background ions, resulting in very little sensitivity of the parallel emission structure on the background plasma flows. This is illustrated by a comparison between simulated CIII TVC 1-D parallel emission profiles for a pair of plumes generated under conditions typical of this region, as shown in Figure 16. In both simulations the jet model is employed. However, in one case (solid curve) no parallel flow is included in the simulation, while in the other case (dashed) a parallel Mach number of -0.18 (constant over the emission volume) is specified. Nonetheless, in both cases the parallel profiles are very similar, and very symmetric.

The results are quite different for simulations conducted with input conditions typical of the far SOL. A comparison between CIII TVC 1-D parallel emission profiles for a pair of plumes generated under such conditions is shown in Figure 17. For both cases the sputter source model is employed. The solid curve represents the case with no parallel flow, and the dashed curve a case with $M_{||}$ = -0.16 (constant over the emission volume). The parallel emission profile is very symmetric when no flow is included, but a significant parallel asymmetry appears in the plume formed under conditions of background plasma flow. These results are consistent with the experimental observations for plumes generated in the far SOL. They also indicate that only in the far SOL can plume emission structure be used to infer the parallel flow velocity.

Finally, studies were conducted to determine the sensitivity of the simulated plume structure to values for the parallel Mach number under conditions typical of the far SOL. Results show that a 20% variation in $M_{||}$ can lead to a $\geq$ 50% variation in the computed parallel plume asymmetry (as deduced from the ratio of LHS and RHS slopes in the 1-D parallel emission profile; see Figure 10). This suggests that the uncertainty in the parallel Mach number inferred from simulation of a given experimental plume will be primarily related to the uncertainty in the value for the parallel asymmetry of the plume, which for typical emission data is of order $\simeq$ 10%.

6. Plasma Flows in the SOL

6.1. Jet-inferred $\boldsymbol{E} \times \boldsymbol{B}$ flows

For plumes generated in the near SOL, the local radial electric field (averaged over a radial extent of $\simeq$ 5 mm) can be inferred from the cross-field deviation of impurity ions

present in the jet (i.e. the jet boomerang angle), since the parallel velocity of these ions can be deduced from the ridge-line analysis. However, it is also necessary to consider the effect of radial variations in the local ionization rate in such an analysis, since these variations may also contribute to the measured boomerang angle. To assess their effect, a simple 1-D Monte Carlo code was developed which approximates the radial density distribution arising from the existence of finite n_e and T_e gradients at the gas injection location. The boomerang angle which results from this distribution was then determined by including effects of parallel ion transport. More details on this calculation can be found in reference [14]. Results indicate that boomerang angle corrections due to effects of ionization rate variation are small ($\simeq 1°$). Nonetheless, these corrections are accounted for in the analysis.

Measurements of the radial electric field based on analysis of CIII TVC plume data in the near SOL ($\mathbf{E}_{r,plume}$) have been performed for a number of ohmic L-mode discharges. These results were then compared both to estimates of $\mathbf{E}_r$ obtained from the radial gradient of the plasma potential profile inferred from scanning probe measurements ($\mathbf{E}_{r,ps}$), and to estimates of the $\mathbf{E} \times \mathbf{B}$ velocity obtained from scanning probe measurements of the poloidal propagation velocity of edge plasma fluctuations ($v_{\mathbf{E}\times\mathbf{B},pf}$) [4]. In the latter case the comparison between plume and probe results is made by converting plume-inferred values of the radial electric field to $\mathbf{E} \times \mathbf{B}$ velocities ($v_{\mathbf{E}\times\mathbf{B},plume}$) using the local value of the magnetic field strength.

A comparison between $\mathbf{E}_{r,plume}$ and $\mathbf{E}_{r,ps}$ is shown in Figure 18 for a number of ohmic L-mode discharges. The discharge conditions span the range of line-average densities from 0.8×10^{20} m$^{-3} < \bar{n_e} < 2.4 \times 10^{20}$ m^{-3}, plasma currents from 0.5 MA $< \mathbf{I}_p <$ 1.0 MA, and toroidal magnetic fields from 4 T $< \mathbf{B}_\phi <$ 6 T. For each discharge considered, $\mathbf{E}_{r,ps}$ data are plotted from *each full probe scan* in ρ-space, whereas $\mathbf{E}_{r,plume}$ values are generated only at the peak insertion of the FSP (i.e. during plume formation). In addition, data are included from probe scans when no gas was injected (i.e. when no plume was formed). Some of the variation in $\mathbf{E}_r$ values obtained from the probe measurements can be related to the different discharge conditions [4]. The probe results also exhibit systematic variations with background plasma conditions (e.g. with plasma density) which are not observed in the plume data. Nonetheless, the results indicate that values of radial electric field inferred from the two measurements are of the same magnitude. However, the radial variation of the inferred $\mathbf{E}_r$ profiles is different. For example, while values for $\mathbf{E}_{r,plume}$ are observed to be positive over the full SOL ($\rho > 0$), indicating that $\mathbf{E}_r$ only changes sign inside the separatrix, data from the FSP suggest that the radial electric field changes sign in the SOL, near $\rho \sim$ 1-3 mm. In addition, $\mathbf{E}_r$ profiles measured by the scanning probe exhibit a steeper gradient near the separatrix relative to the plume-inferred results. However, this apparent discrepancy may be a result of the lack of plume data near the separatrix. Nonetheless, the comparison between $\mathbf{E}_{r,plume}$ and $\mathbf{E}_{r,ps}$ suggests the possibility of an error in either the plume or probe measurements.

Comparisons between $v_{\mathbf{E}\times\mathbf{B},plume}$ and $v_{\mathbf{E}\times\mathbf{B},pf}$ for the same set of discharges are

shown in Figure 19. For each discharge considered, $v_{\mathbf{E}\times\mathbf{B},pf}$ data are plotted from *each full probe scan* in ρ-space, whereas $v_{\mathbf{E}\times\mathbf{B},plume}$ values are generated only at the peak insertion of the FSP (i.e. during plume formation). Data are also included from probe scans in which no gas was injected (i.e. when no plume was formed). As before, the probe results exhibit systematic variations with background plasma conditions which are not observed in the plume data. In addition, the sparse set of plume data points near $\rho \leq 0$ does not allow a clear comparison to be made between plume and probe results in this region. Nonetheless, both the magnitude and the radial variation of the $\mathbf{E} \times \mathbf{B}$ velocity profile is similar for the plume and probe measurements in this case.

It is clear from Figures 18 and 19 that the two methods of inferring radial electric field from the probe ($\mathbf{E}_{r,ps}$, $v_{\mathbf{E}\times\mathbf{B},pf}$) do not agree. The plume measurements suggest that $\mathbf{E}_{r,ps}$ is unreliable near the separatrix; this method appears to get the sign of $\mathbf{E}_r$ wrong in this region. On the other hand, $v_{\mathbf{E}\times\mathbf{B},pf}$ yields positive values of $\mathbf{E}_r$ over the entire SOL, a result more consistent with the plumes. In reference [4] it was concluded that if $v_{\mathbf{E}\times\mathbf{B},pf}$ is a reliable measure of the radial electric field then the total plasma flow pattern in the SOL near the midplane is dominated by a pure toroidal rotation. The plume measurements lend some support to this hypothesis.

Estimates for the radial electric field have also been made for plumes formed during EDA H-mode. Plume emission has been generated both inside and outside of the Quasi-Coherent (QC) mode layer, and results for the plume boomerang angle suggest that the radial electric field changes sign inside the mode layer (see Figure 4). Using ridge-line analysis, the values of $\mathbf{E}_r$ are estimated to be 4.3 kV/m outside of the mode layer (ρ = 3.6 mm) and -3.3 kV/m inside of the mode layer (ρ = 1.2 mm). In this case, radial electric field values inferred from a probe-sheath model are 5.1 kV/m and 5.4 kV/m outside and inside of the QC mode layer, respectively. These results indicate that probe measurements do not get the sign of $\mathbf{E}_r$ correct in the mode layer, suggesting that plumes may provide the only means of measuring radial electric field in this region. In addition, the plume results suggest a strong radial electric field gradient in the vicinity of the QC mode, of order $\sim$ 3 V/mm^2.

6.2. Parallel flows in the far SOL

Plumes generated in the far SOL are simulated using the sputter source model, since the recycling-induced density perturbation is expected to be small in this region. In addition, the parallel Mach number ($M_{||}$) is assumed to be constant over the emission volume (on field lines outside of the probe presheath). The value of $M_{||}$ inferred from simulation of the parallel plume asymmetry is therefore a volume-averaged quantity.

For conditions typical of the far SOL, the simulated CIII parallel plume extent is found to be quite sensitive to inputted values for the electron temperature. This is primarily a result of the sharp variation in the C^{+2} ionization lifetime with T_e under these conditions. Simulation studies indicate that an increase in the temperature profile of 25% can result in a reduction of the simulated CIII parallel plume extent by $\sim$ 50%.

This sensitivity suggests that simulation of the CIII parallel plume extent may provide a cross-calibration for electron temperature measurements made by the scanning probe.

Asymmetries in the parallel plume extent are expected to be sensitive to parallel asymmetries of electron density and temperature in the presheath zones under conditions typical of the far SOL. Density and temperature asymmetries, which are indeed observed in the probe measurements, are in turn thought to result from the shorter connection length for field lines on the downstream side of the probe (i.e. field lines connected to the outer divertor) relative to the upstream side. In principle, the parallel mean-free path of impurity ions will differ on either side of the probe due to n_e and T_e asymmetries (since the ionization lifetime will differ), which can lead to a parallel asymmetry in the impurity emission even in the absence of a background parallel flow. However, results arising from these effects are thought to be small, since the asymmetries only occur on field lines in the probe presheath. In fact, results from simulation studies indicate that the effect of including these asymmetries is a modification in the parallel plume asymmetry by only $\sim$ 10-15% (for typical values of the asymmetry, e.g. $n_{e,up}/n_{e,down} = T_{e,up}/T_{e,down} = 1.8$). This suggests that uncertainties in the plume-inferred values of $M_{||}$ resulting from the presence of parallel density and temperature asymmetries are of the same order (i.e. $\sim$ 10-15%).

Setting $U_0 = 5$ eV and $\lambda_{ss} = 1$ cm in the sputter source model, LIM has been used to extract volume-averaged values of the parallel Mach number from plume data generated in the far SOL for both a normal and reversed field discharge. Results from this analysis for the normal field discharge are shown in Figure 10. To obtain a match between simulation and experiment for this case, it was necessary to increase the electron temperature profile inputted into the simulation uniformly by 25% relative to measurements from the scanning probe. For these conditions, the inferred Mach number was found to be $M_{||} = 0.18$, which is significantly lower than the value measured by the probe for this discharge (= 0.46; calculated using Equation 1).

To simulate the experimental plume generated during reversed field operation, it was necessary to decrease the electron temperature profile inputted into the simulation uniformly by 25% relative to measurements from the scanning probe. In this case, the inferred Mach number was found to be $M_{||} = 0.21$. This is again significantly lower than the value measured by the probe for this discharge (= 0.59; calculated using Equation 1).

One possible explanation for the discrepancy between plume-inferred and probe-inferred values of $M_{||}$ is the small field line connection length on the downstream side of the scanning probe. Equation 1 is based on a probe presheath model in which the field line connection lengths upstream and downstream are both much larger than the presheath connection length. On the upstream side of the probe this criterion is always met, whereas on the downstream side of the probe this criterion is not satisfied in the far SOL. A consequence of this result is lower electron density on the downstream side, which leads to a larger value for the probe-inferred Mach number. Thus, it is possible that low density on the downstream side of the probe, and not a strong parallel flow, is responsible for the large values of $M_{||}$ inferred from the probe measurements. This

suggests that it may be necessary to use a more sophisticated Mach probe theory, i.e. one which corrects for effects of small field line connection length relative to presheath connection length (such as [25]), in the analysis of probe data from the far SOL plasma.

Additional causes for the discrepancy between plume and probe results include measurement errors by the probe and/or the use of an inappropriate parallel flow model in the simulation, the latter of which suggests that a more sophisticated model of background plasma flows in the far SOL may be necessary in LIM. Nonetheless, the value for the plume-inferred parallel Mach number is found to be larger in the reversed field discharge relative to the normal field discharge, which is consistent with general probe results. The results also imply that, if anything, the (FSP) Mach probe overestimates the flow towards the divertor in the far SOL, which strengthens the argument for the main-chamber recycling view of scrape-off layer particle balance in Alcator C-Mod [7].

7. Summary

Results from experiments and modelling of impurity transport in response to a localized gas-puff in the SOL of Alcator C-Mod are reported. Deuterated ethylene, C_2D_4, is injected through the end of a reciprocating fast-scanning probe. The resultant emission ("plume") is imaged from two near-perpendicular views using coherent fiber bundles optically coupled to gated, intensified CCD cameras through beam-splitters, allowing for the simultaneous acquisition of C^{+1} and C^{+2} plume data at each view location. With this unique system, impurity dispersal has been studied over the full range of the scrape-off layer (up to the separatrix) in a divertor tokamak for the first time.

Plume structure is observed to depend on local values of electron density and temperature, background parallel flow, and radial electric field. Emission resulting from sputtering of carbon deposited on the probe surface also contributes to the structure. For plumes generated in the near SOL, emission contours are non-elliptical and the parallel extent relative to the ionization mean-free path is large, indicating a local "jetting" of impurities along $\mathbf{B}$. Plume results also suggest an elongation of the impurity ion density down the probe axis.

A Monte Carlo impurity transport code (LIM) was used to simulate the 3-D structure of the plumes. Results indicate that contributions to the emission from sputtering explain the cross-field plume width, and that the parallel extent of emission generated in the far SOL is well-described using a sputter launch-energy distribution for the impurities. In the near SOL, the presence of a localized parallel electric field arising from background ion recycling off the probe surface is necessary to explain the parallel extent of emission generated in this region. This electric field accelerates impurity ions formed near the probe tip away from the probe, causing jet-like behavior. LIM was also used to investigate causes for the vertical elongation of the impurity emission. Results suggest the existence of a probe-induced $\mathbf{E} \times \mathbf{B}$ drift, of order $\sim$ 1000 m/s in the near SOL. This drift may be responsible for the transport of both impurity and bulk plasma

ions down the probe axis.

Values for $v_{||}$ in the far SOL and $\mathbf{E}_r$ in the near SOL have been extracted from the plume structure. A comparison between plume and probe results for $\mathbf{E}_r$ from a number of ohmic L-mode discharges suggests that calculations which employ a probe-sheath model may be in error, and that measurement of the poloidal propagation velocity of edge plasma fluctuations may be a more reliable means of inferring $\mathbf{E}_r$ from probe data. Plumes have also been used to estimate the radial electric field during Enhanced D_α H-mode, and results indicate both that $\mathbf{E}_r$ is negative inside the Quasi-Coherent mode layer and that the radial electric field gradient in this region is large ($\sim$ 3 MV/m^2). Finally, comparisons between plume- and probe-inferred values for the parallel Mach number suggest that the probe over-estimates parallel flow to the divertor in the far SOL, where effects of short field line connection to the divertor are important. This result strengthens the argument for the main-chamber recycling view of particle balance in the Alcator C-Mod SOL.

Acknowledgements

These results were made possible by the excellent engineers, technical staff, scientists and students on the Alcator team. The authors would especially like to thank Dr. Stewart Zweben at the Princeton Plasma Physics Laboratory for the loan of a CCD camera and coherent fiber bundle for use in these experiments, Dr. Ricardo Maqueda at Los Alamos National Laboratory for the loan of a CCD camera for use in these experiments, Josh Stillerman at Alcator C-Mod for his efforts setting up and developing software for the plume imaging data acquisition system, Dr. Cyrus MacLatchy at Acadia University for his efforts developing software for virtual imaging of the simulated results, Yi-Jung Yang at Kutztown University for her assistance with data organization and analysis, Dr. David Elder and Steven Lisgo at the University of Toronto for their assistance with LIM modelling, and Prof. Ian Hutchinson at Alcator C-Mod for his advice, support and counsel. This work is supported by US Department of Energy Contract no. DE-FC02-99-ER-54512.

References

[1] LaBombard, B. *et al* 1997 *Journal of Nuclear Materials* **241–243** 149
[2] Asakura N. *et al* 1999 *Nucl. Fusion* **39** 1983
[3] Coad J.P. *et al* 2001 *Journal of Nuclear Materials* **290–293** 224
[4] LaBombard B., Gangadhara S., Lipschultz B., and Pitcher C.S. 2003 *Journal of Nuclear Materials* **313–316** 995
[5] Chankin A.V. 1997 *Journal of Nuclear Materials* **241–243** 199
[6] Stangeby P.C. 2000 *The Plasma Boundary of Magnetic Fusion Devices* (Philadephia: Institute of Physics Publishing) p 298
[7] LaBombard B. *et al* 2000 *Nucl. Fusion* **40** 2041
[8] Pitcher C.S., Stangeby P.C., Goodall D.H.J., Matthews G.F., and McCracken G.M. 1989 *Journal of Nuclear Materials* **162–164** 337
[9] Matthews G.F. *et al* 1990 *Proceedings of the 18th European Conference on Controlled Fusion and Plasma Physics* vol **III** p 229
[10] McCracken G.M. *et al* 1990 *Journal of Nuclear Materials* **176–177** 191
[11] Weschenfelder F. *et al* 1996 *Plasma Physics and Controlled Fusion* **38** A311
[12] Jablonski D. 1996 *Local Gas Injection as a Scrape-off Layer Diagnostic on the Alcator C-Mod Tokamak* (Cambridge:M.I.T.) PhD thesis
[13] LaBombard B. *et al* 1999 *Journal of Nuclear Materials* **266–269** 571
[14] Gangadhara S. 2003 *Physics and Application of Impurity Plume Dispersal as an Edge Plasma Flow Diagnostic on the Alcator C-Mod Tokamak* (Cambridge:M.I.T.) PhD thesis
[15] Hutchinson I.H. 1988 *Physical Review A* **37** 4358
[16] Lao L.L., St. John H., and Stambaugh R.D. 1985 *Nucl. Fusion* **25** 1611
[17] Stangeby P.C., Farrell C., Hoskins S., and Wood L. 1988 *Nucl. Fusion* **28** 1945
[18] Snipes J.A. *et al* 2001 *Plasma Physics and Controlled Fusion* **43** L23
[19] Greenwald M. *et al* 1999 *Physics of Plasmas* **6** 1943
[20] LaBombard B. 2002 *Physics of Plasmas* **9** 1300
[21] van Goubergen H. *et al* 1999 *Plasma Physics and Controlled Fusion* **41** L17
[22] Langley R.A. *et al* (editors) 1984 *Data Compendium for Plasma-Surface Interactions (Nucl. Fusion Special Issue)* (Vienna: IAEA) p 61
[23] Janev R.K., Langer W.D., Evans Jr K., and Post Jr D.E. 1987 *Elementary Processes in Hydrogen-Helium Plasmas* (New York: Springer-Verlag)
[24] Roth J., Vietzke E., and Haasz A.A. 1991 *Atomic and Plasma Material Interaction Data for Fusion* **1** 63
[25] Hutchinson I.H. 1991 *Physics of Fluids B* **3** 847

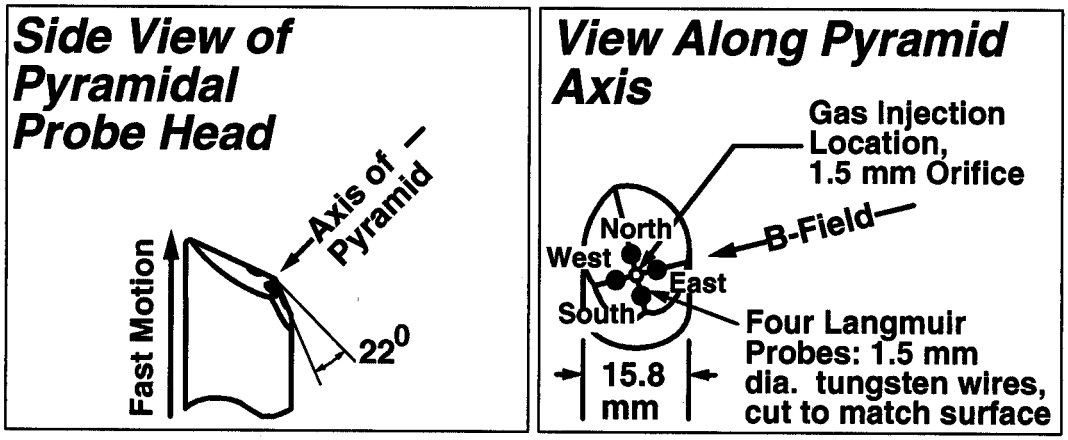

Figure 1. Close-up views of gas-injecting scanning probe (actual scale). The probe head is made from molybdenum, the wires which serve as Langmuir probes from tungsten, and the capillary tube and inertial valve from stainless steel. The Langmuir probes are oriented to have directional sensivity both along and across **B**, yielding information on local SOL flows in addition to values for electron density and temperature.

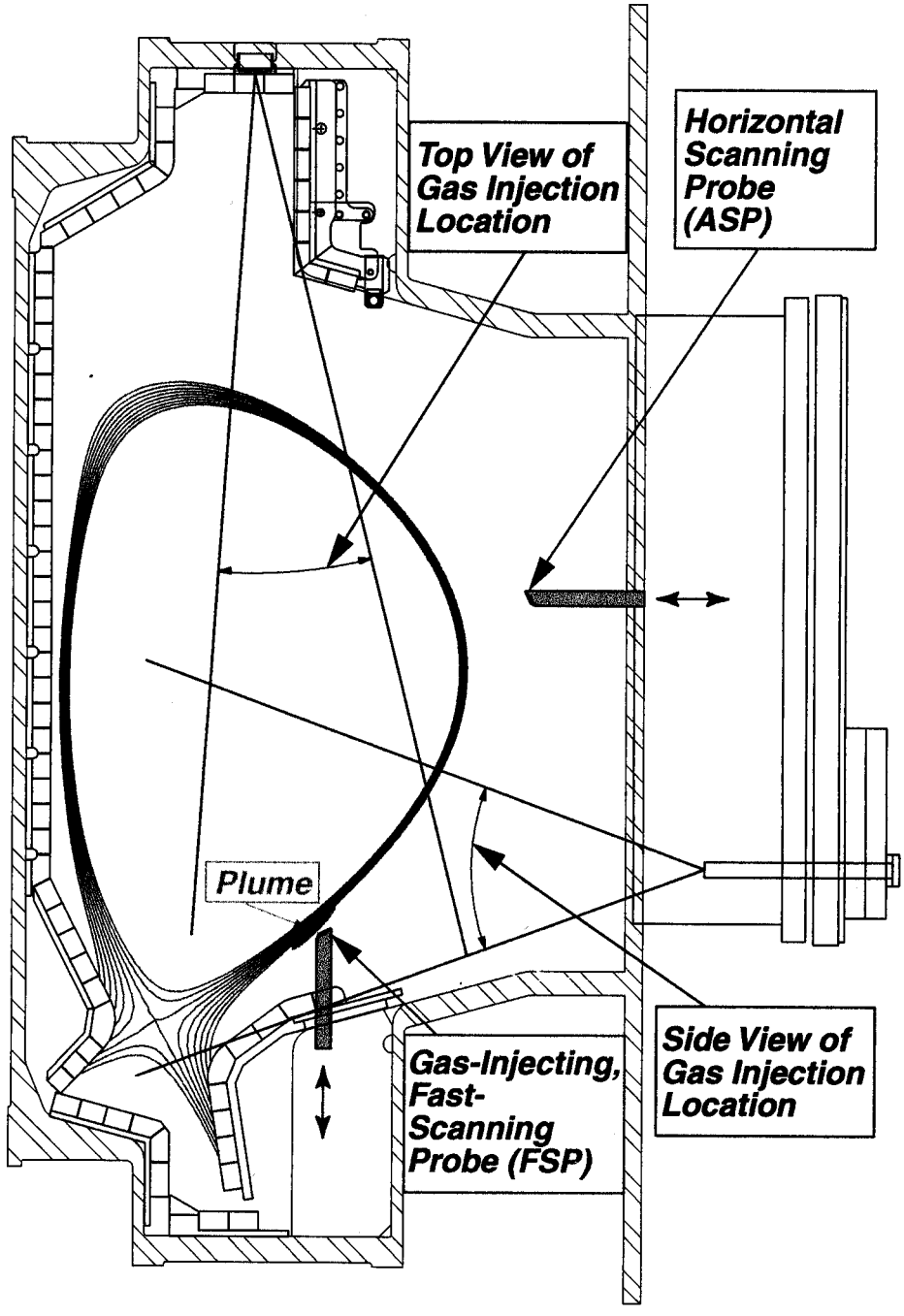

Figure 2. Cross-section of the Alcator C-Mod vacuum chamber with a typical diverted equilibrium. Gas is injected at the end of stroke of a vertically-scanning probe (FSP). Impurity emission plumes are viewed from two near-perpendicular locations. Measurements of background plasma conditions in the SOL are available from both the FSP as well as a horizontal fast-scanning probe located slightly above the outboard midplane (ASP).

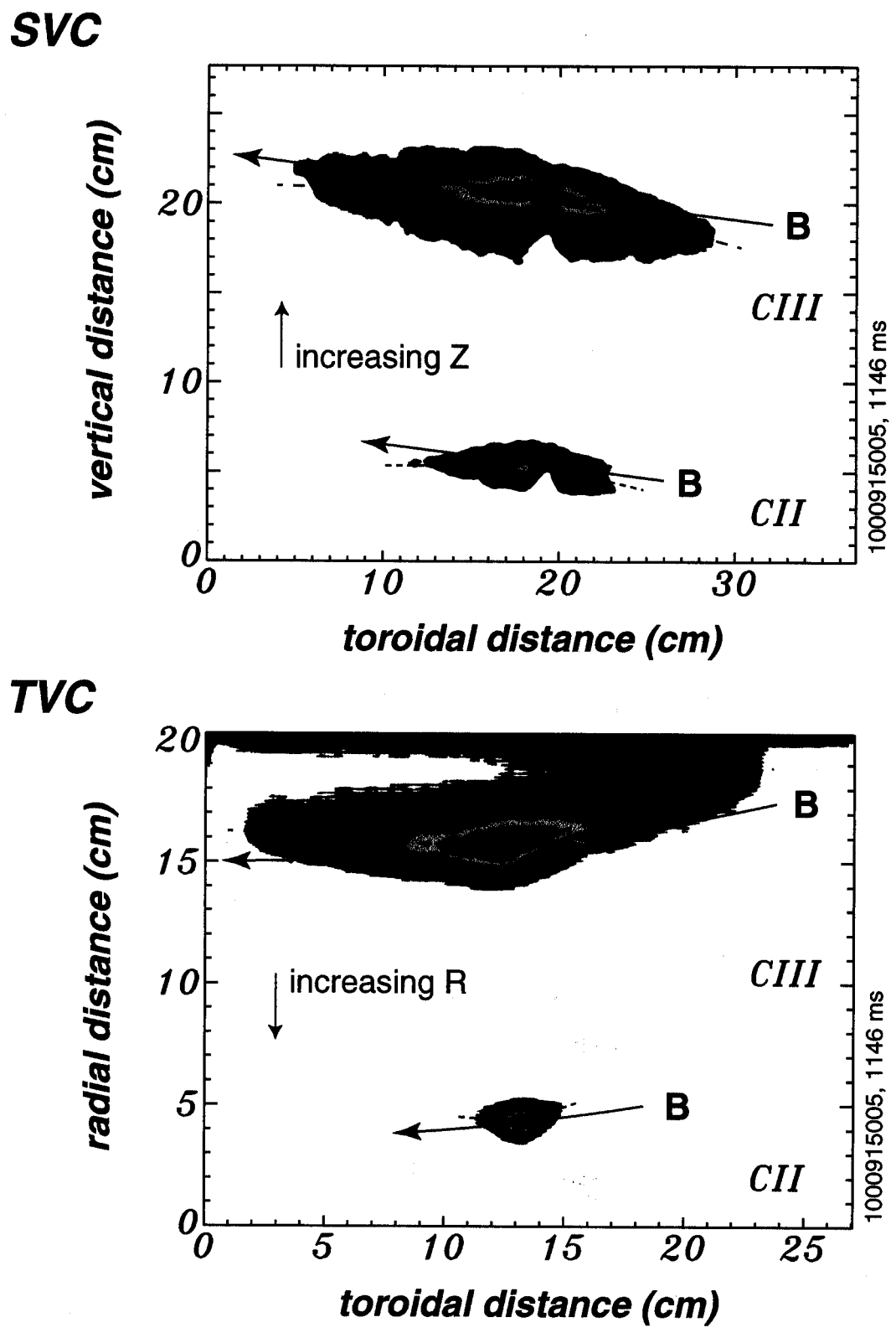

Figure 3. Typical data obtained from plume imaging system, side (*top panel*) and top (*bottom panel*) view. In both cases emission from C^{+1} is on the bottom half of the image and emission from C^{+2} is on the top half. Note: Raw image with 9×9 pixel smoothing.

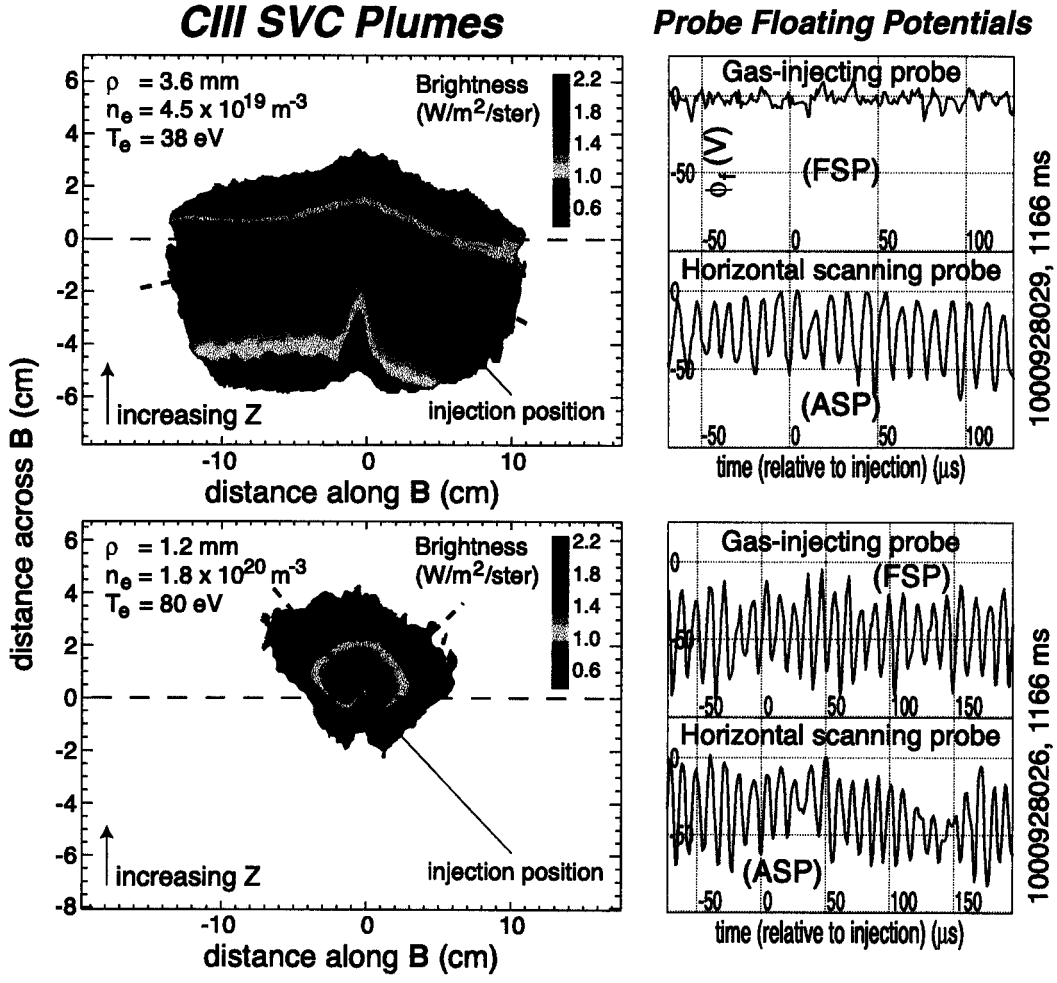

Figure 4. Comparison between CIII SVC plumes generated inside and outside of the Quasi-Coherent (QC) mode layer during a pair of Enhanced D_α (EDA) H-mode discharges. Floating potential measurements from the gas-injecting scanning probe (FSP) and the horizontal fast-scanning probe (ASP) are also shown. Results suggest that the QC mode exists in a region of $\mathbf{E}_r < 0$. Note: Images are 9×9 pixel smoothed, absolutely calibrated, and mapped to field-aligned coordinates.

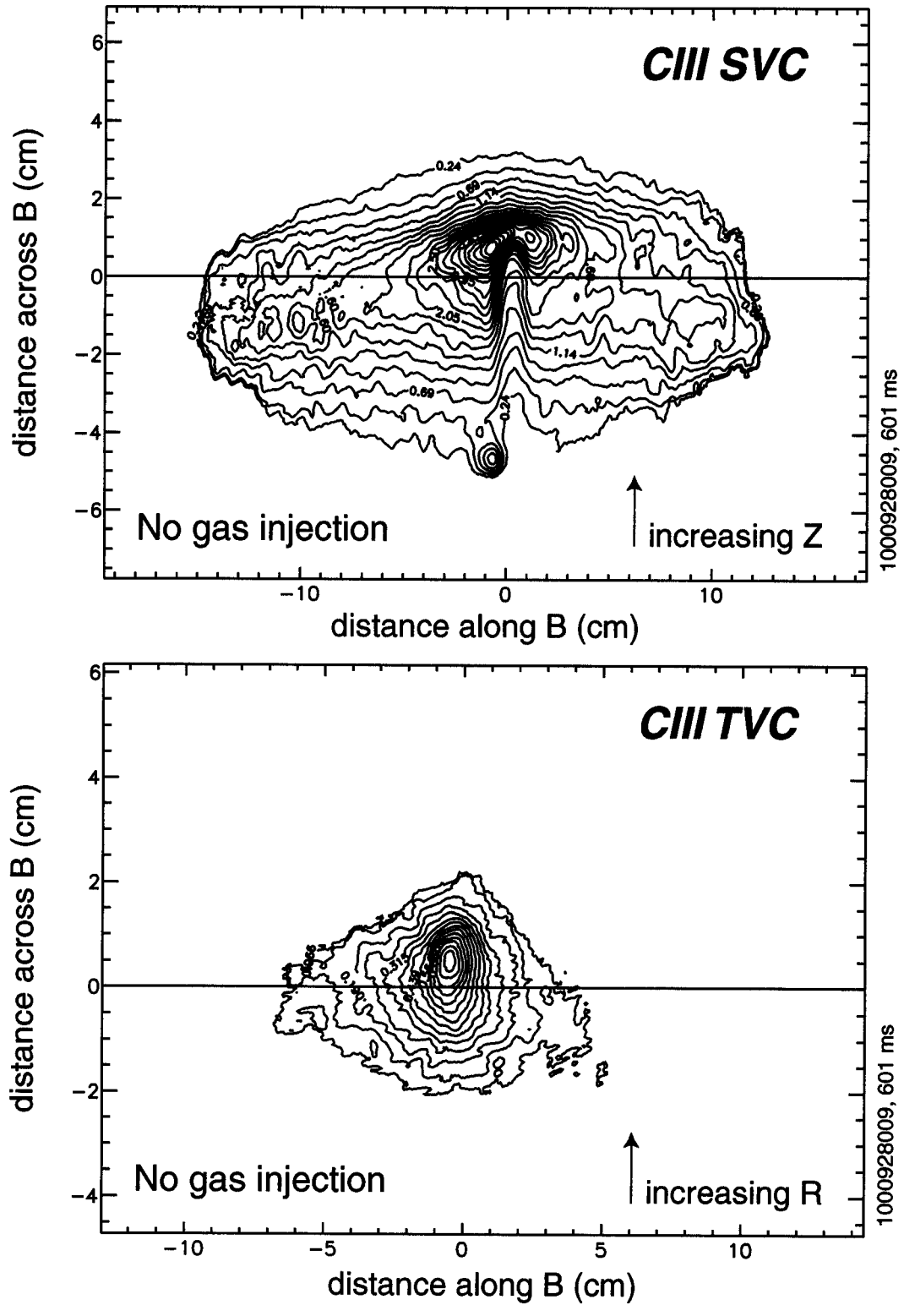

Figure 5. Data obtained from plume imaging system for a case with *no gas injection*, side (*top panel*) and top (*bottom panel*) view. Contours are labeled in units of brightness ($W/m^2/ster$). The plume is thought to be formed from sputtering of re-deposited carbon off the probe head. Note: Images are 9×9 pixel smoothed, absolutely calibrated, and mapped to field-aligned coordinates.

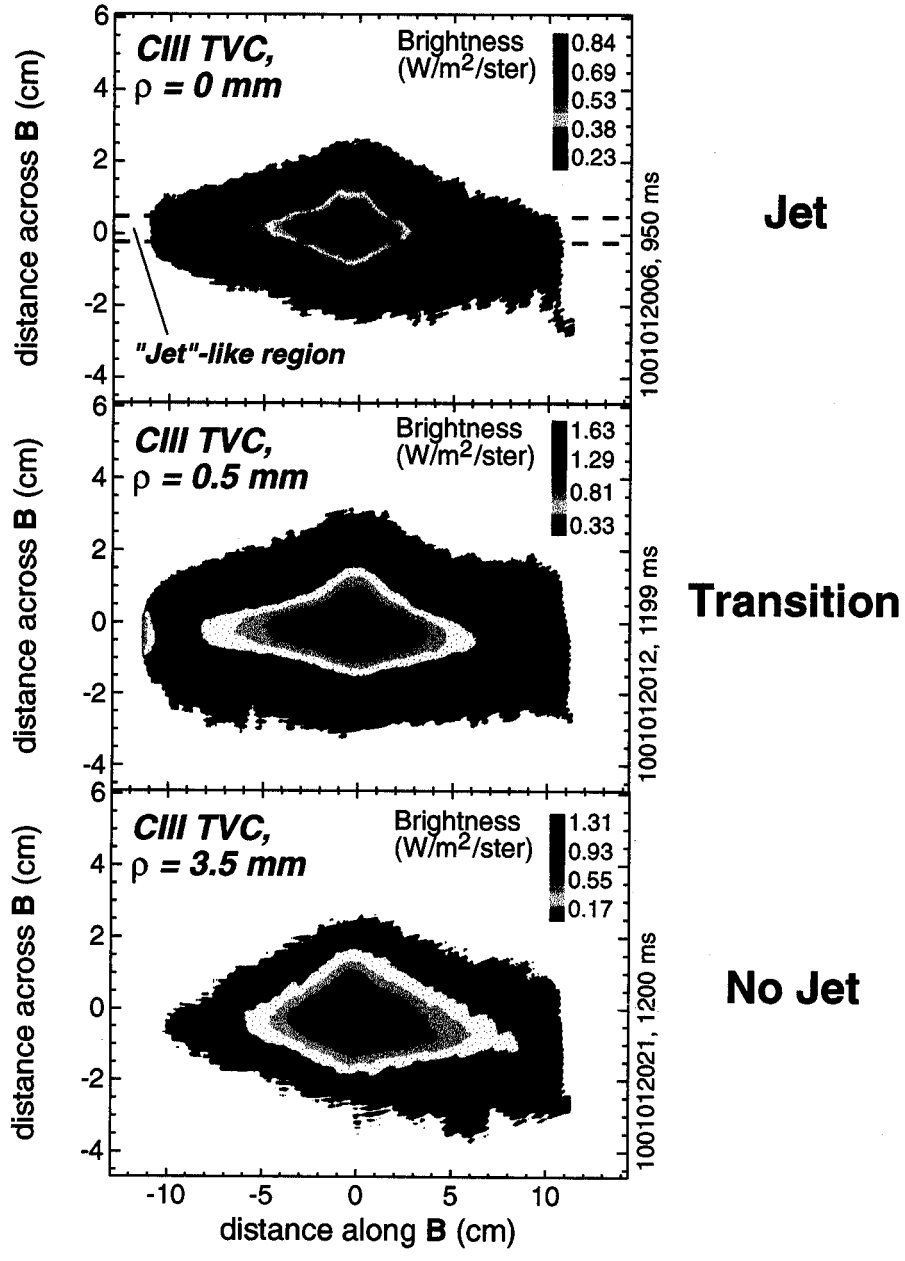

Figure 6. *Top panel:* CIII TVC image of a plume generated in the near SOL. The plume exhibits a "jet"-like structure, leading to non-elliptical emission contours. *Middle panel:* Example of a CIII TVC image which exhibits weak jet behavior, and is therefore labeled as a "transition" plume. *Bottom panel*: Example of a CIII TVC image which exhibits no jet-like behavior. The emission contours are nearly elliptical in this case, consistent with results from a single-source model for the plumes (i.e. formation due to sputtering only).

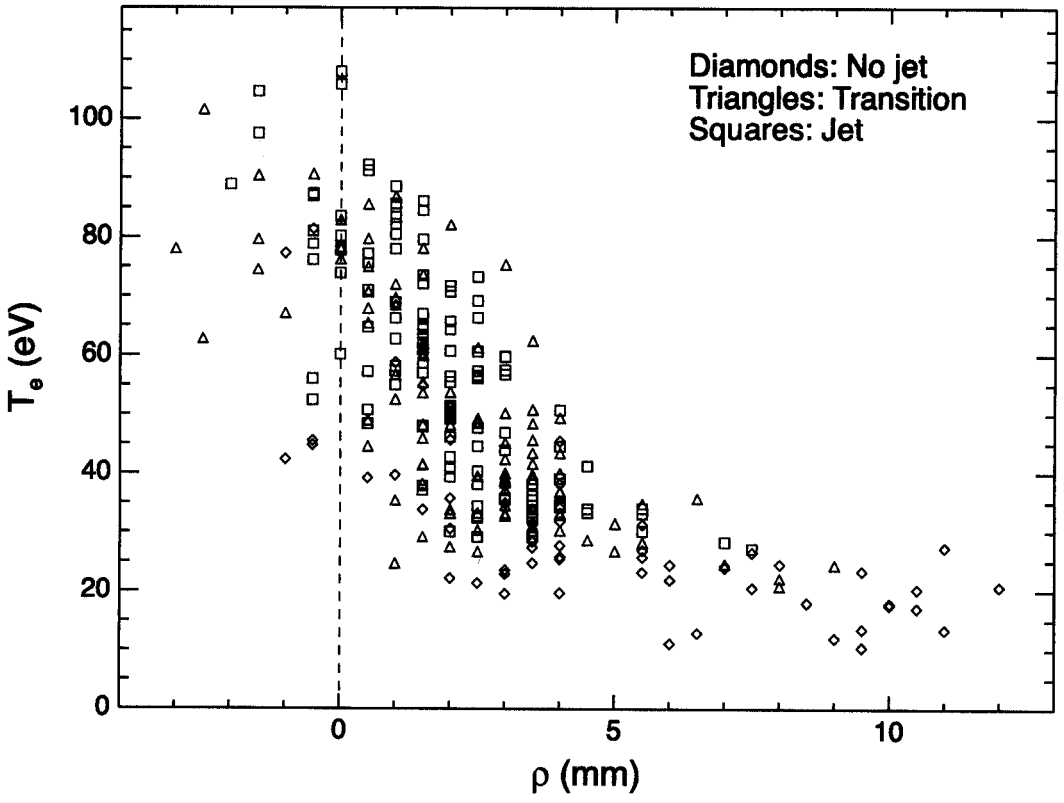

Figure 7. Plot of electron temperature (as measured by the FSP) vs. SOL depth for all discharges in which plumes were formed. Points are sorted based on a qualitative categorization regarding the degree of "jetting" in the emission. These results indicate that "jet"-like behavior predominantly occurs close to the separatrix, i.e. at high values of T_e.

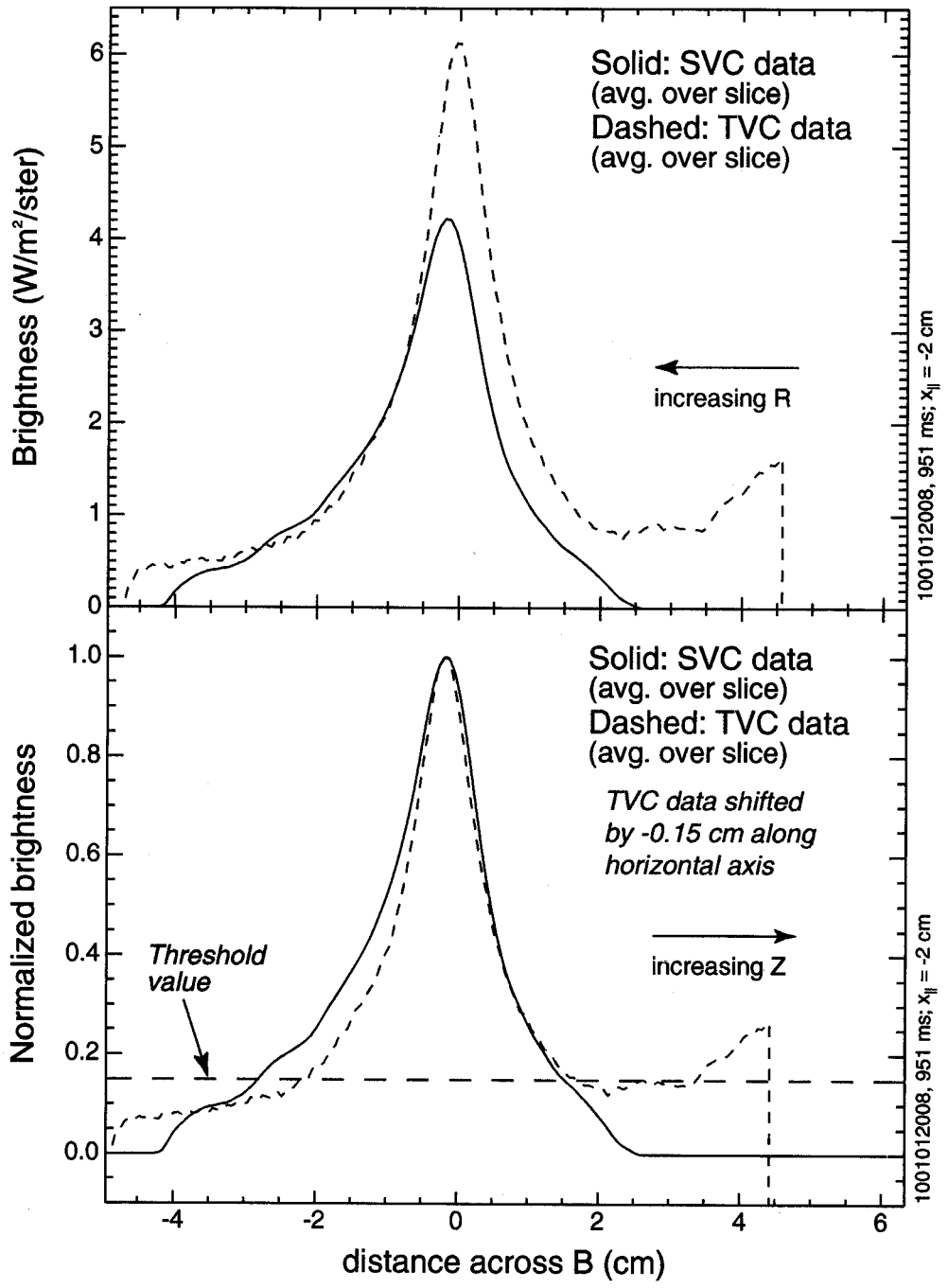

Figure 8. Comparisons between CIII SVC and TVC 1-D cross-field brightness profiles for a plume formed in the near SOL. *Top panel:* Absolute brightness profiles calculated from integration of the 2-D brightness data over a limited parallel extent. *Bottom panel:* Normalized brightness profiles. Neglecting data in the far field, the SVC profile appears skewed relative to the TVC profile, confirming that the plume is vertically elongated.

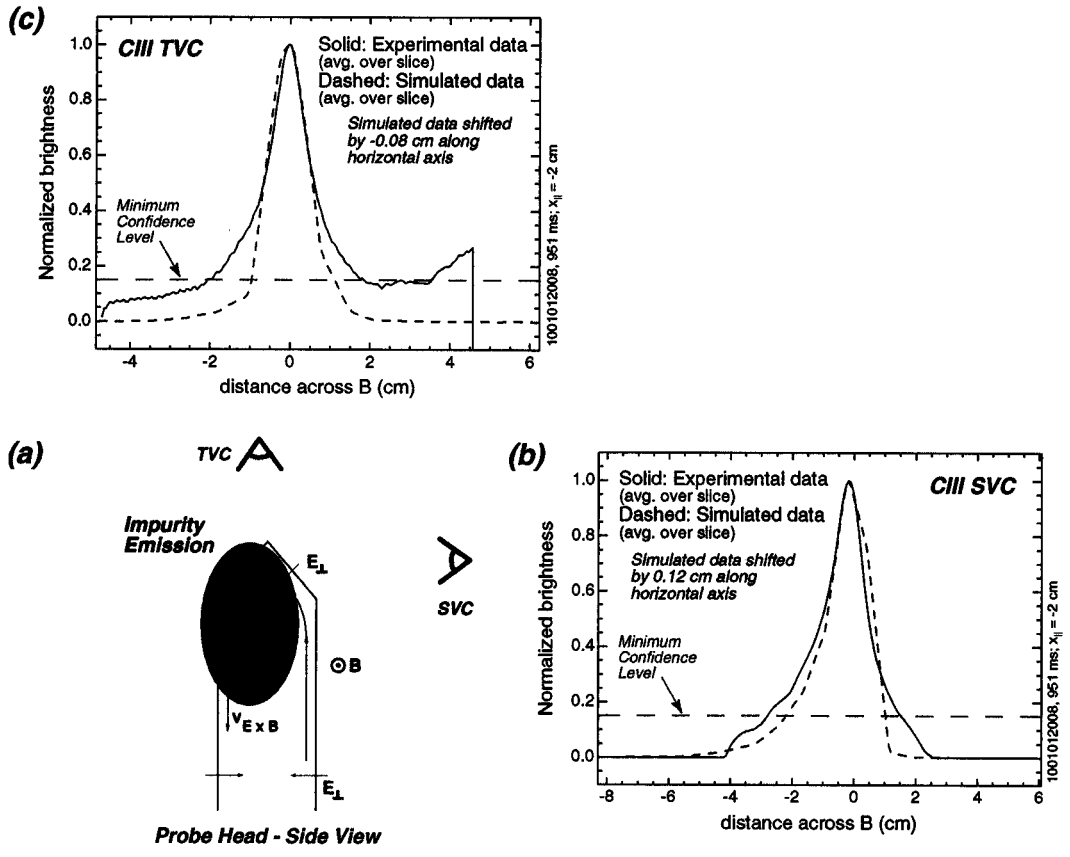

Figure 9. (*a*) Schematic of the probe geometry indicating the direction of the electric field which results from variations in plasma potential near the probe surface, the direction of the resultant $\mathbf{E} \times \mathbf{B}$ drift, and the possible effect of such a drift on the impurity ion distribution. (*b,c*) Comparison between simulated and experimental 1-D cross-field profiles of normalized brightness for the SVC and TVC (experimental data are the same as in Figure 8). A vertical impurity ion drift has been included in the simulation, and the electron density has been assumed constant in the calculation of the emission excitation rate. Relatively good agreement is observed between simulation and experiment for both the profile width and profile skewness in this case (when considering data above a minimum confidence level).

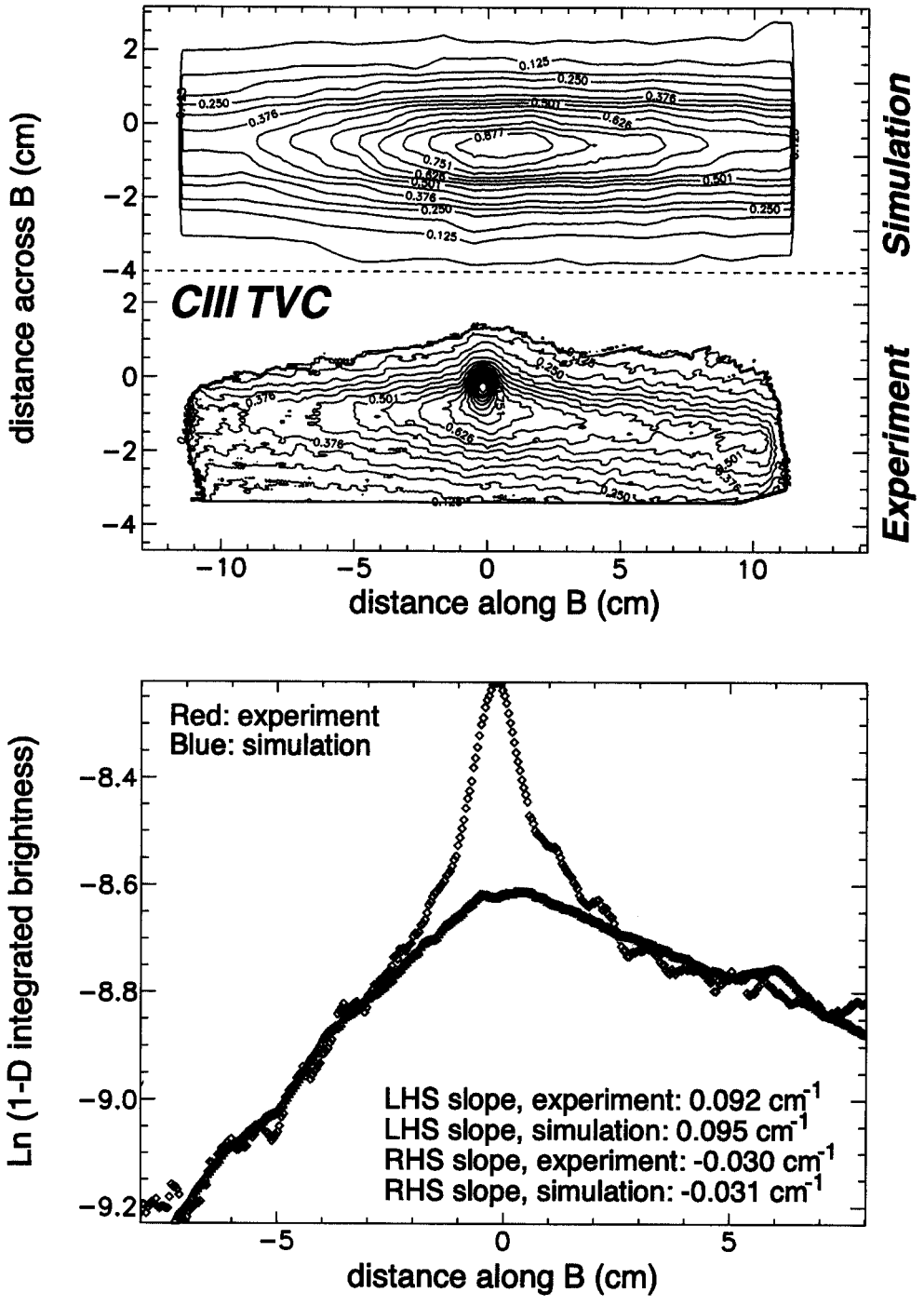

Figure 10. *Top panel:* Comparison between experimental and simulated 2-D CIII TVC plumes in the far SOL, for normal field operation. Good agreement is observed between values for the cross-field plume width, which are within 12% in this case. *Bottom panel:* Comparison between 1-D parallel emission profiles for plumes shown above. Close to the injection, reflections off the probe head result in the experimental emission being peaked. However in the far field inverse decay lengths are approximately equal for experiment and simulation. The parallel Mach number inferred from the plume simulation is $M_{||} = 0.18$ in this case, which is significantly lower than the value measured by the scanning probe for this discharge (= 0.46, calculated using Equation 1).

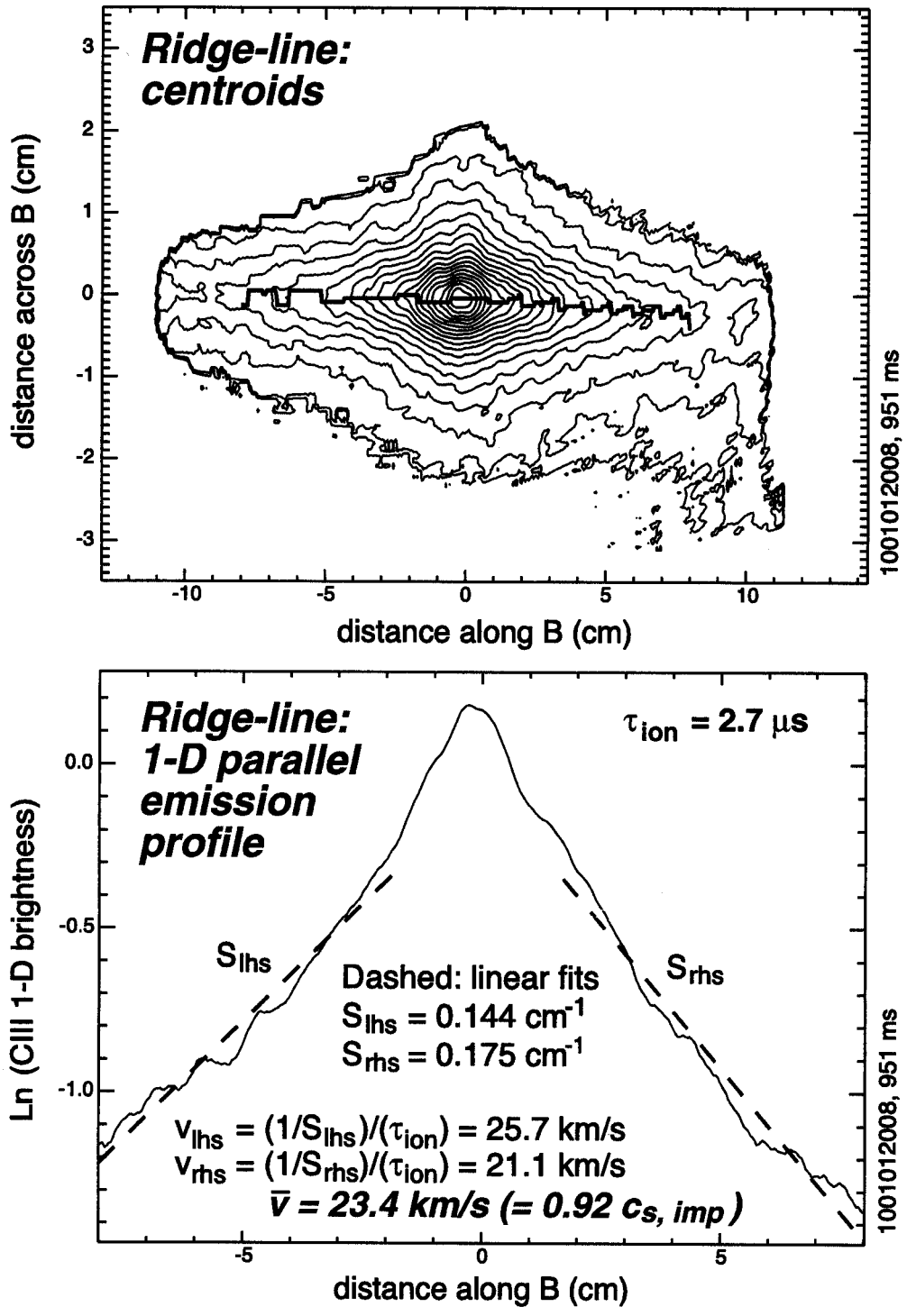

Figure 11. An example of "ridge-line" analysis for a CIII TVC plume. Centroids (*top panel*) are determined at each parallel coordinate by finding the location of the peak in the corresponding 1-D cross-field profile. The value of the brightness at this peak is then used to fill in the 1-D parallel emission profile array (*bottom panel*). Slopes which are obtained on either side of the injection location (S_{lhs}, S_{rhs}) from a linear fit to the emission profile (in semi-log space) characterize the parallel extent of the plume, and are used to estimate the average parallel velocity of the impurity ions in the jet ($\bar{v} = (v_{lhs} + v_{rhs})/2$). For plumes generated in the near SOL this velocity can be large, of order the impurity ion sound speed ($c_{s,imp}$).

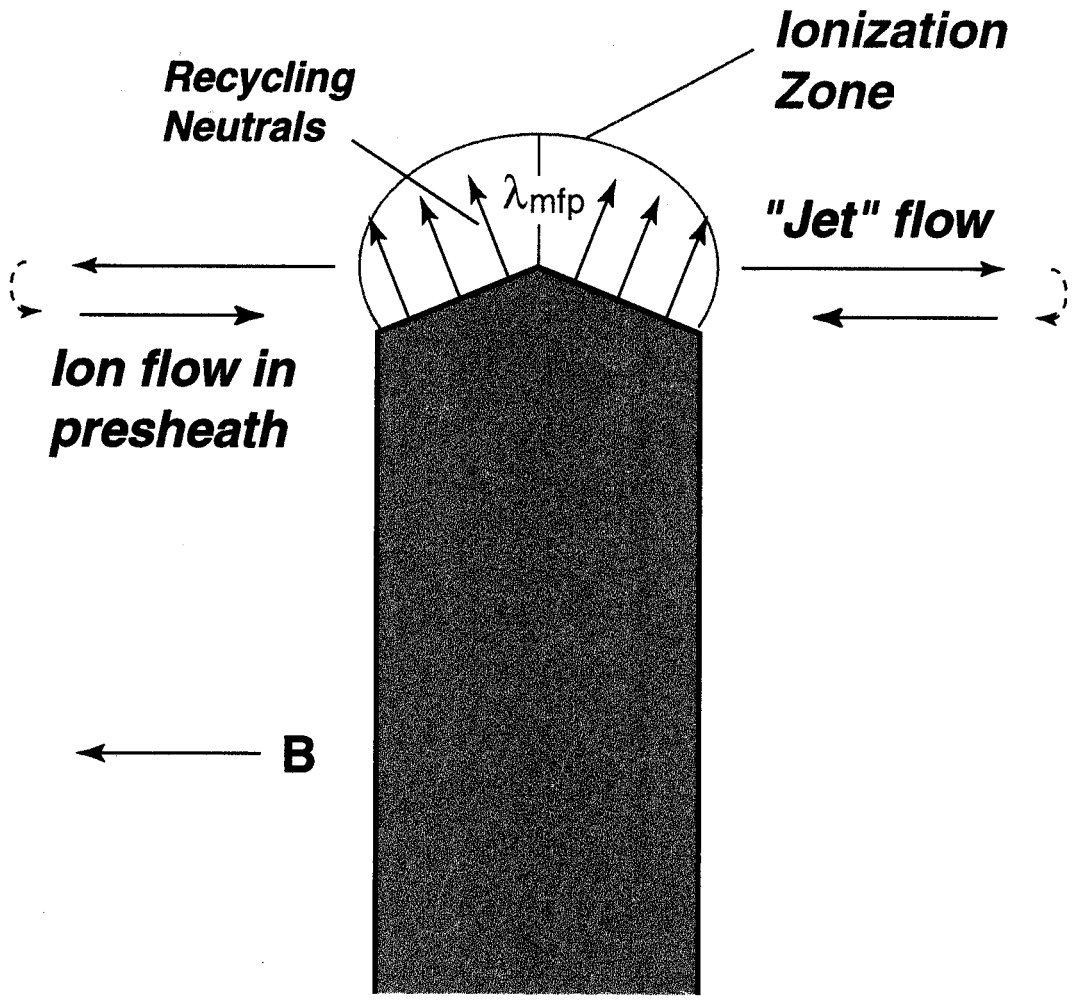

Figure 12. Schematic illustrating the process of background ion recycling off the probe surface. Neutrals formed by recycling appear predominantly on field lines outside the presheath, and ionize in a volume determined by local plasma conditions (n_e, T_e). This local ionization results in the formation of a density perturbation, which is thought to be responsible for causing the impurity ion jet.

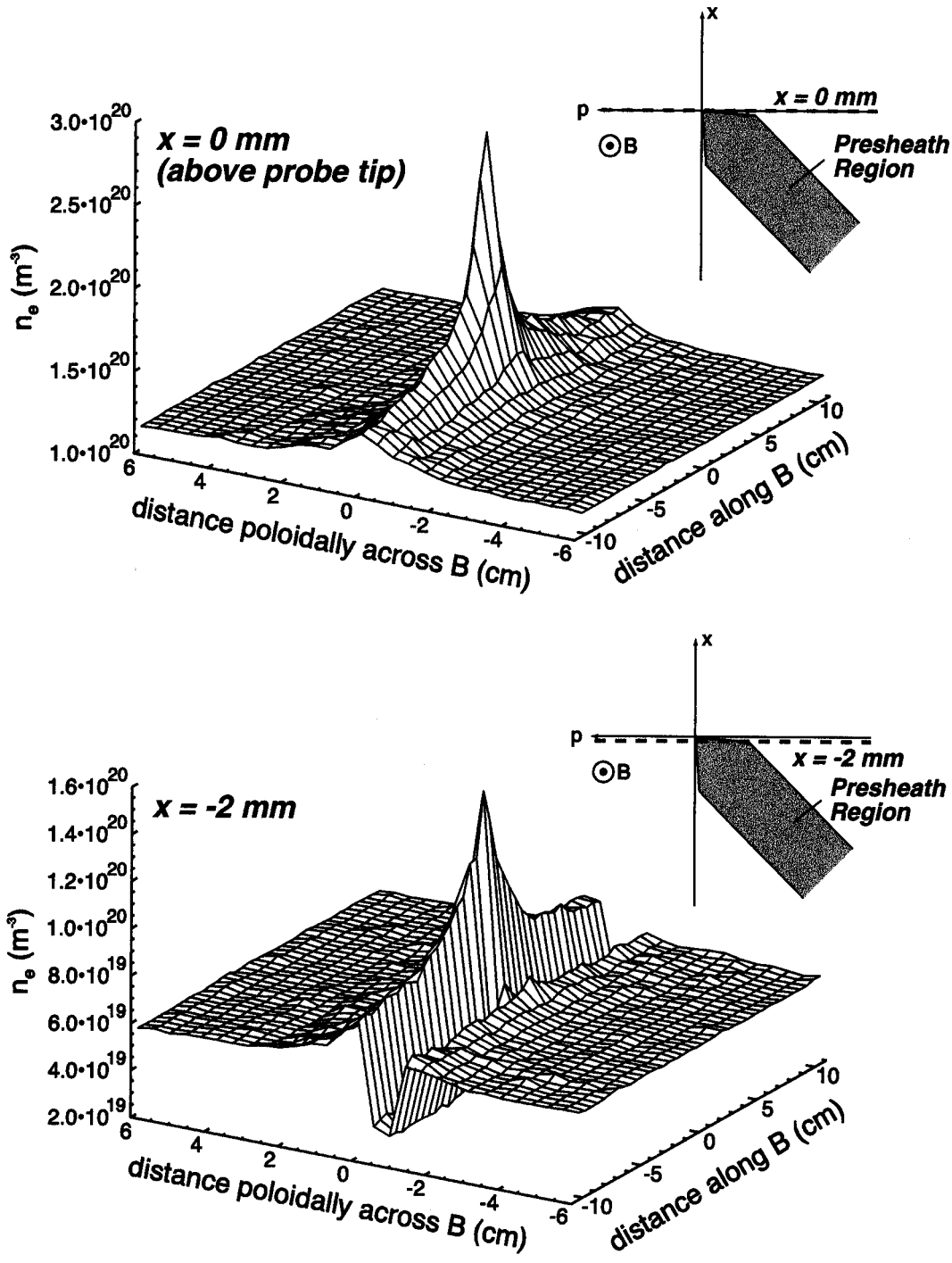

Figure 13. Surface plots of the total electron density (background plus recycling-induced) at two radial coordinates: x = 0 mm (*top panel*) and x = -2 mm (*bottom panel*). Background density and temperature profiles typical of the near SOL were used as inputs, and a recycling rate of 2.6 × 10^{20} atoms/second is assumed. Effects arising from density variation in the presheath have also been included. The density is peaked in the poloidal coordinate, suggesting that the recycling perturbation occurs predominantly on field lines near (but not connected to) the probe surface.

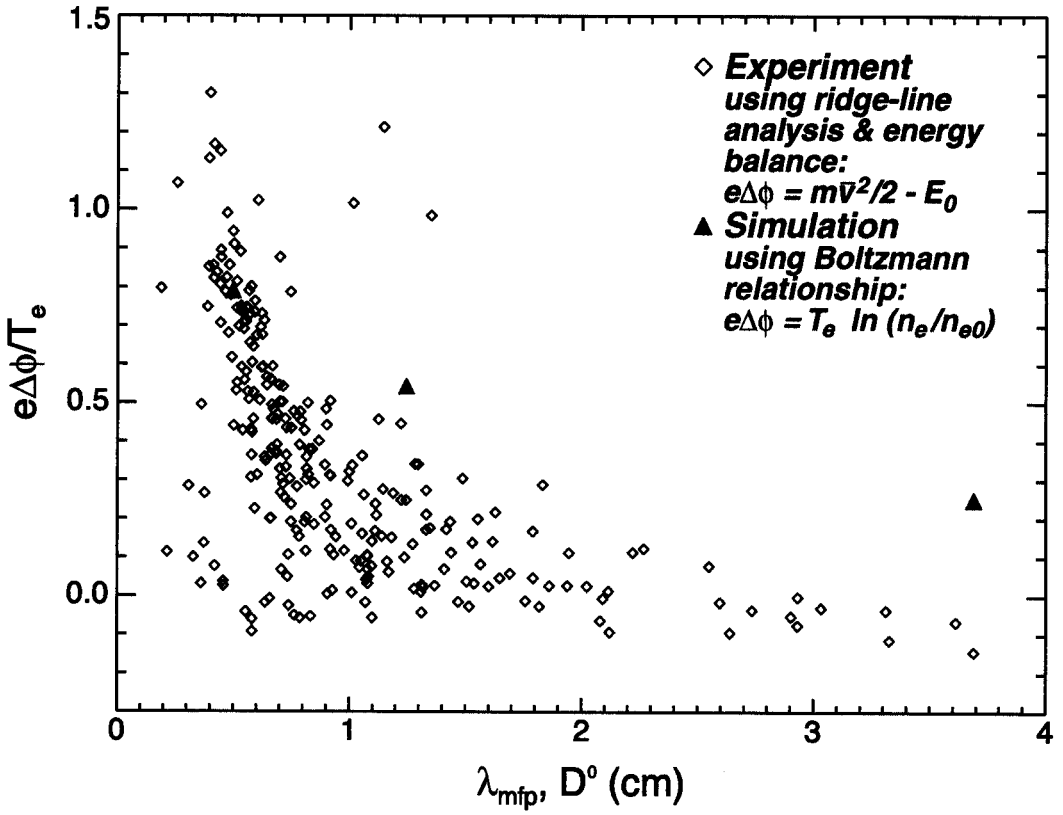

Figure 14. Plot of the normalized potential drop vs. ionization mean-free path for deuterium neutrals recycling from the probe surface. The experimental results (*diamonds*) suggest a strong relationship between potential drop and mean-free path, whereas simulation results (*triangles*) indicate a weaker dependence. Nonetheless, the general trends are similar, and there is good agreement for results in the near SOL (i.e. at small λ_{mfp}).

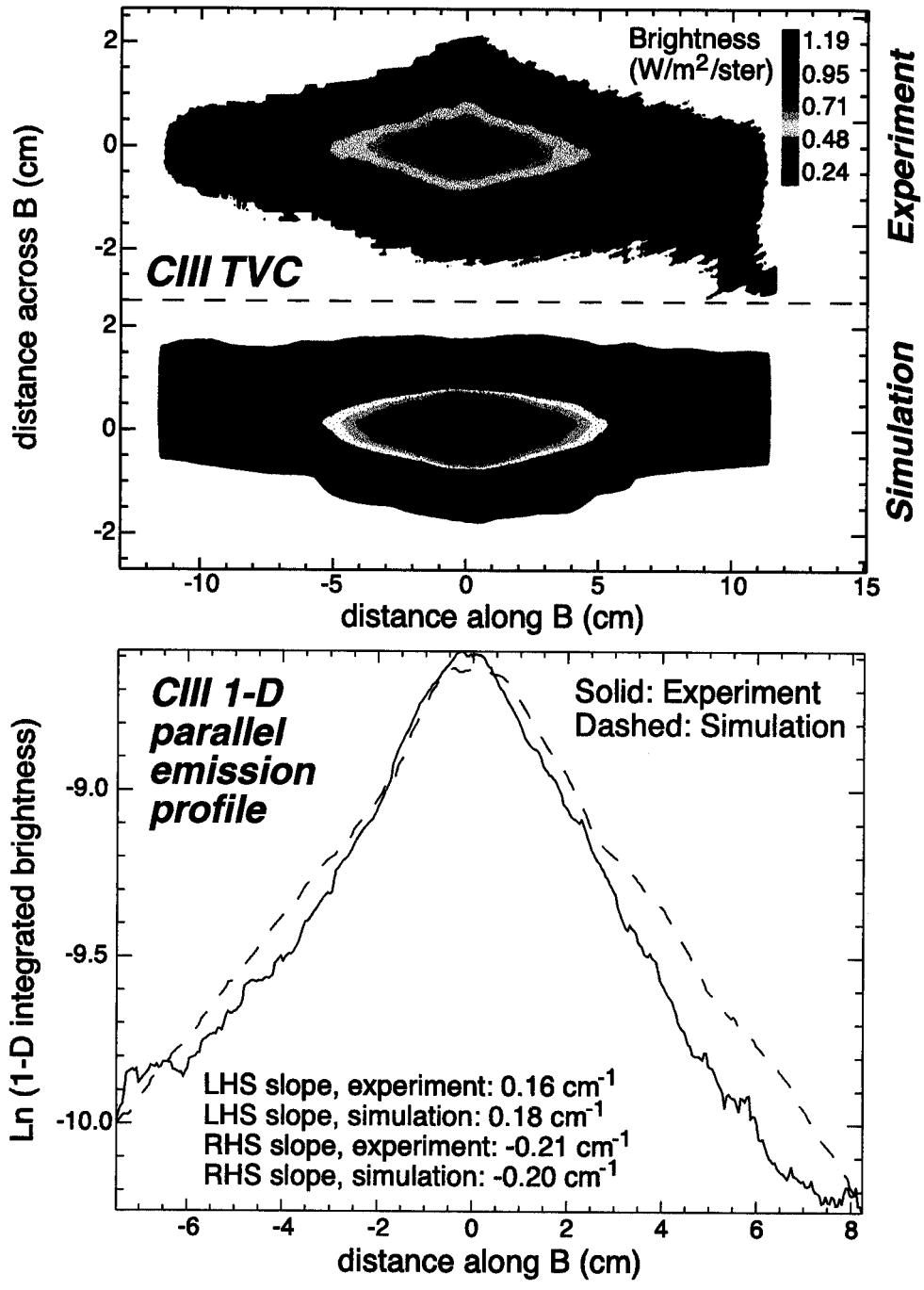

Figure 15. *Top panel:* Comparison between experimental CIII TVC plume generated in the near SOL and a composite CIII TVC simulation plume generated by summing together (with equal weight) emission components arising from a localized impurity launch into a background plasma containing the recycling-induced parallel electric field and from a sputter source launch into a nominal (no $E_{\parallel,pert}$) plasma background. In this case both the cross-field width and the parallel extent of the emission compare reasonably well with the experimental results. *Bottom panel:* Comparison between experimental and simulated 1-D parallel emission profiles for the plumes shown above. Values for the inverse decay lengths are found to agree within $\simeq$ 10%.

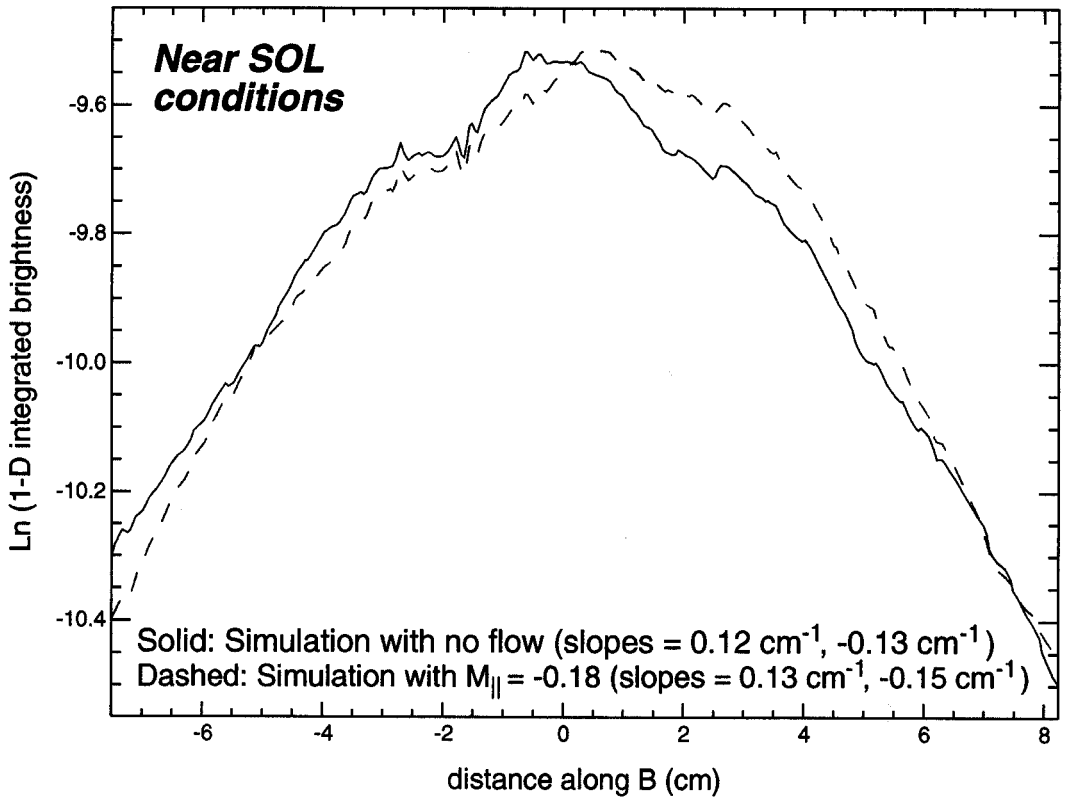

Figure 16. Comparison between simulated CIII TVC 1-D parallel emission profiles for cases with (dashed curve) and without (solid) background plasma flow. In both cases the jet model is employed, and density and temperature profiles characteristic of the near SOL are used. Profiles are similar for both cases, and very symmetric, indicating that background plasma flows have very little influence on the parallel structure of plumes formed in the near SOL.

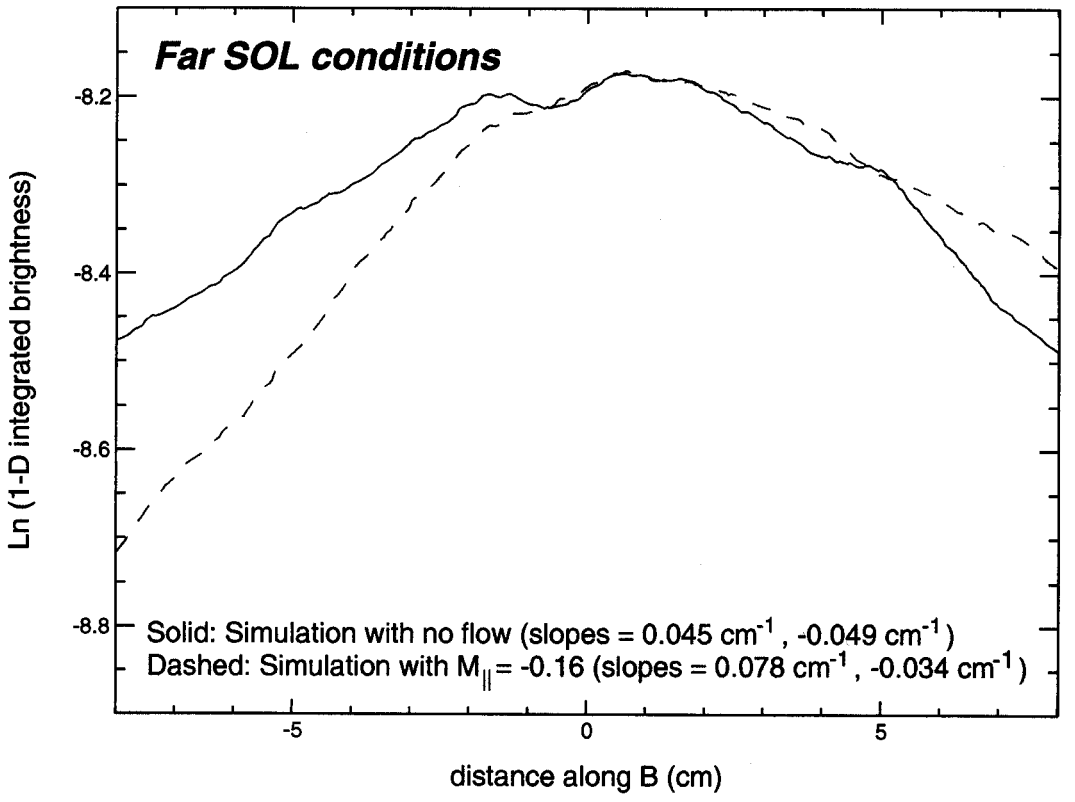

Figure 17. Comparison between simulated CIII TVC 1-D parallel emission profiles for cases with (dashed curve) and without (solid) background plasma flow. In both cases the sputter source model is employed, and density and temperature profiles characteristic of the far SOL are used. The profiles are very different for the two cases: with no flow, the profile is very symmetric, while with flow included the profile exhibits a strong asymmetry. These results are consistent with the experimental observations for plumes generated in the far SOL.

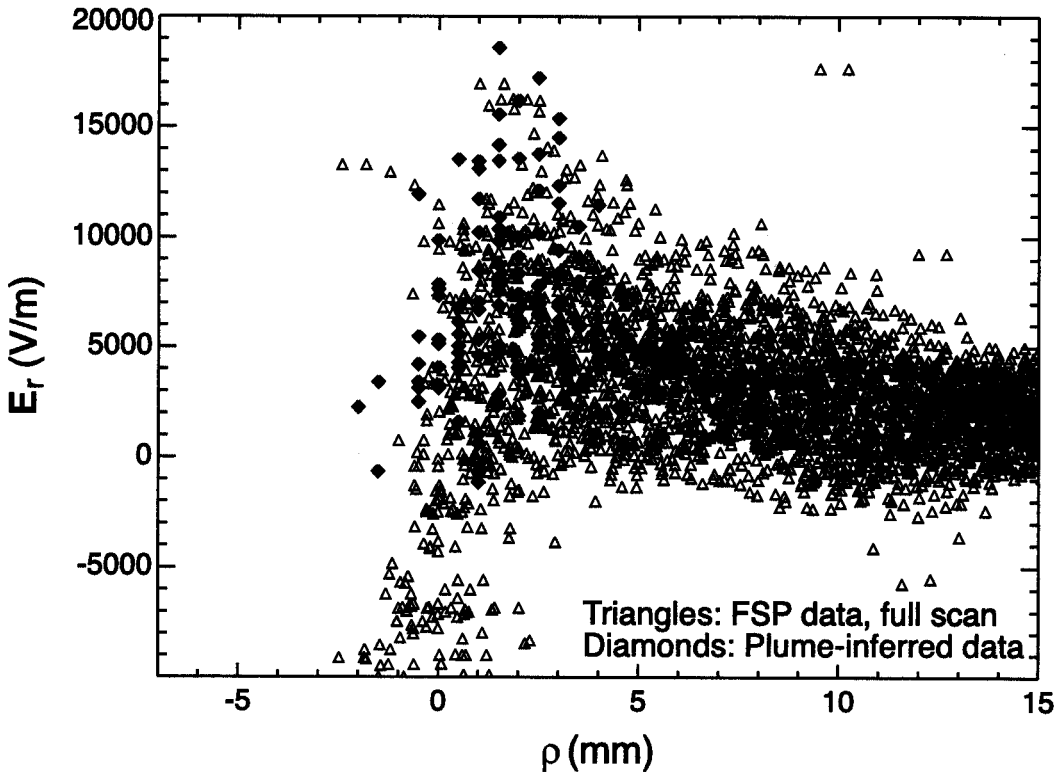

Figure 18. Comparison between radial electric field values obtained from plume data and probe data for a number of ohmic L-mode discharges. The latter values are calculated from the radial gradient of the inferred plasma potential. Results indicate that values of $\mathbf{E}_r$ inferred from the two measurements are of the same magnitude, but that the radial variation of the inferred $\mathbf{E}_r$ profiles is different. This suggests the possibility of an error in either the plume or probe measurement.

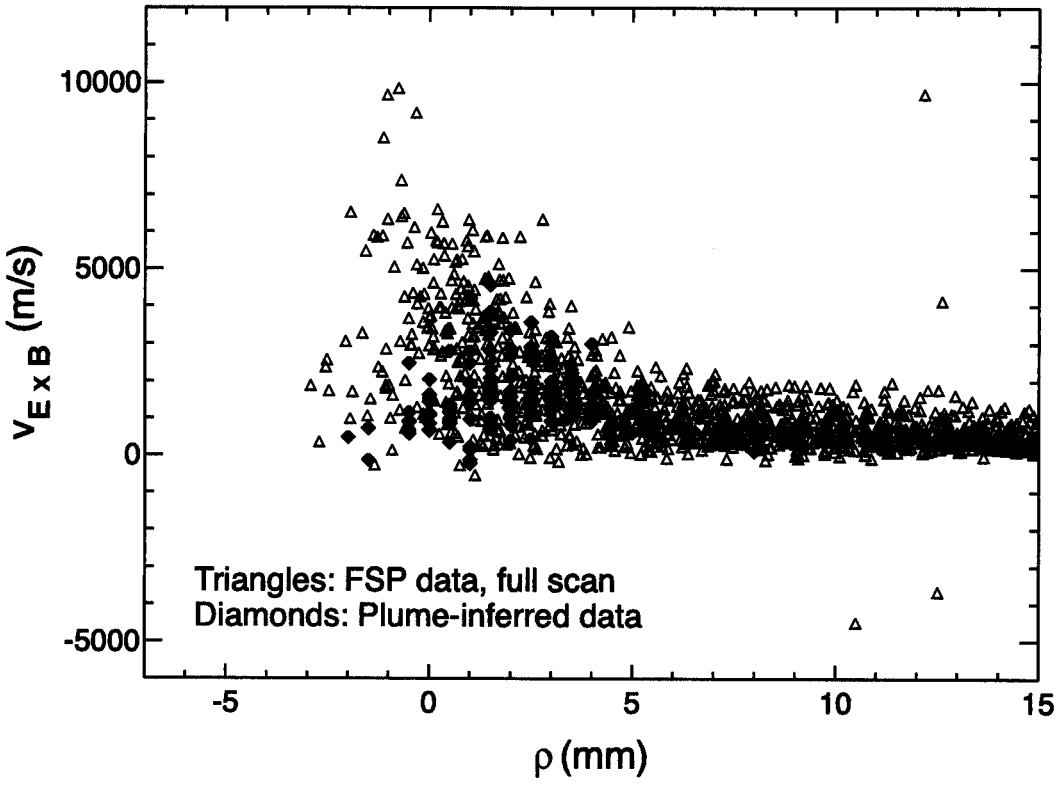

Figure 19. Comparison between $\mathbf{E} \times \mathbf{B}$ velocities obtained from plume data and probe data for a number of ohmic L-mode discharges. The latter values are calculated from the poloidal propagation velocity of edge plasma fluctuations [4]. Good agreement exists between the two measurements for both the magnitude of $v_{\mathbf{E}\times\mathbf{B}}$ as well as the radial variation of the inferred $\mathbf{E} \times \mathbf{B}$ profile. This suggests that measurements of $\mathbf{E}_r$ which employ a probe sheath model may be in error, and that edge plasma fluctuations may provide a more reliable means of determining local values for the radial electric field in the SOL.